Bio-Design and Manufacturing (2023) 6:150–173
https://doi.org/10.1007/s42242-022-00194-3

RESEARCH ARTICLE

Evaluation of different crosslinking methods in altering the properties of extrusion-printed chitosan-based multi-material hydrogel composites

Suihong Liu[1,2,3] · Haiguang Zhang[2,3,4] · Tilman Ahlfeld[1] · David Kilian[1] · Yakui Liu[2] · Michael Gelinsky[1] · Qingxi Hu[2,3,4]

Received: 10 November 2021 / Accepted: 20 February 2022 / Published online: 1 April 2022
© The Author(s) 2022

Abstract

Three-dimensional printing technologies exhibit tremendous potential in the advancing fields of tissue engineering and regenerative medicine due to the precise spatial control over depositing the biomaterial. Despite their widespread utilization and numerous advantages, the development of suitable novel biomaterials for extrusion-based 3D printing of scaffolds that support cell attachment, proliferation, and vascularization remains a challenge. Multi-material composite hydrogels present incredible potential in this field. Thus, in this work, a multi-material composite hydrogel with a promising formulation of chitosan/gelatin functionalized with egg white was developed, which provides good printability and shape fidelity. In addition, a series of comparative analyses of different crosslinking agents and processes based on tripolyphosphate (TPP), genipin (GP), and glutaraldehyde (GTA) were investigated and compared to select the ideal crosslinking strategy to enhance the physicochemical and biological properties of the fabricated scaffolds. All of the results indicate that the composite hydrogel and the resulting scaffolds utilizing TPP crosslinking have great potential in tissue engineering, especially for supporting neo-vessel growth into the scaffold and promoting angiogenesis within engineered tissues.

Graphic abstract

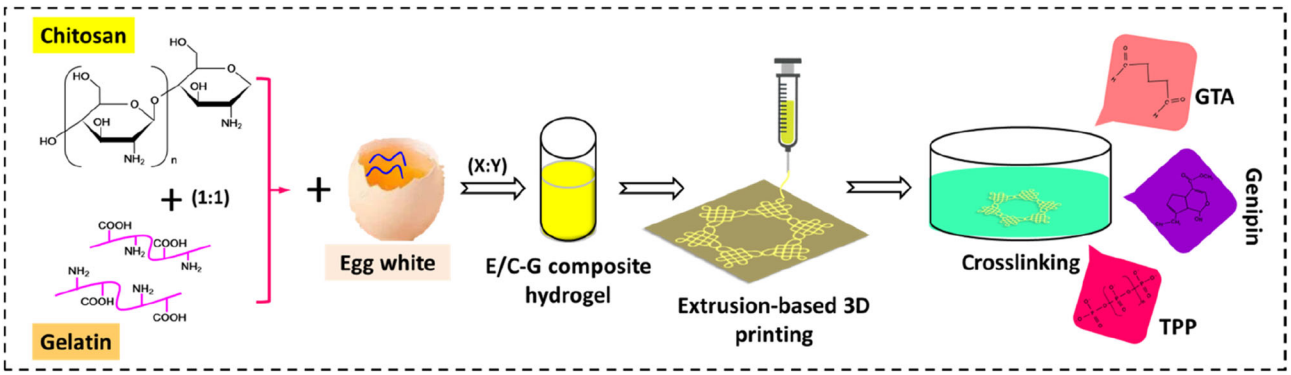

Keywords Multi-material composite hydrogel · Crosslinking mechanism · Chitosan · Gelatin · Egg white · 3D printing

✉ Michael Gelinsky
michael.gelinsky@tu-dresden.de

✉ Qingxi Hu
huqingxi@shu.edu.cn

1 Centre for Translational Bone, Joint and Soft Tissue Research, Faculty of Medicine and University Hospital Carl Gustav Carus, Technische Universität Dresden, 01307 Dresden, Germany

2 Rapid Manufacturing Engineering Center, School of Mechatronic Engineering and Automation, Shanghai University, Shanghai 200444, China

3 Shanghai Key Laboratory of Intelligent Manufacturing and Robotics, School of Mechatronic Engineering and Automation, Shanghai University, Shanghai 200444, China

4 National Demonstration Center for Experimental Engineering Training Education, Shanghai University, Shanghai 200444, China

Introduction

Three-dimensional (3D) printing is an additive manufacturing (AM) process in which successive layers of material are deposited to form volumetric 3D objects with spatially distributed features. This technique has been widely applied in tissue engineering and regenerative medicine [1, 2]. Extrusion-based 3D printing, as one of the most studied AM techniques, can be considered as the most promising and straightforward printing method to fabricate tissue-engineering scaffolds or anatomy-specific 3D shapes due to its adaptability to a broad spectrum of biomaterials [3, 4]. In the past decade, although rapid progress has been witnessed regarding the fabrication of scaffolds, several limitations remain. For instance, selecting suitable materials for scaffolds to provide or support a temporary environment for cell attachment, proliferation, and vascularization has always been a challenge in tissue engineering [5, 6]. Universal single-phase biomaterials were applied in conventional 3D printing, which, in many cases, not only exhibited poor printability and shape fidelity, especially at lower concentrations, but also they failed to meet the biological requirements of cell and tissue growth with respect to the heterogeneity of native tissues and organs [7, 8]. Hence, the development of multi-material hybrid biomaterials applied to 3D printing has been intense, which includes utilizing multiple biomaterials to print hybrid tissue-engineering architecture, in order to accommodate the specific physiological properties of individual tissues.

Hydrogels, as a promising material type, have been widely used for fabricating tissue scaffolds due to their unique advantages such as a high water content, ease of printability, hydrophilicity, and biocompatibility [9, 10]. Various naturally derived materials have been employed to manufacture hydrogel scaffold structures, such as gelatin, alginate, chitosan, agarose, and hyaluronic acid [11, 12]. However, using a single biomaterial among those mentioned above, it is difficult to construct a scaffold that mimics the biomechanical and biochemical properties of native tissue, due to the typically limited printability and effectiveness of crosslinking. Meanwhile, the combination of various biopolymer hydrogels can promote the mechanical, rheological, and biological properties of biomaterials for 3D printing [13]. Therefore, composite hydrogels comprised of two, three or more biomaterials exhibit a great potential for tunable printability and post-printing mechanical and biological properties by varying the initial concentrations of these components. Jiang et al. blended alginate and gelatin to prepare a composite hydrogel with tunable elasticity and biofunctionality by adjusting the material formulation, and thus created 3D breast tumor models [9]. The mechanical integrity of hydrogel materials has proved as a fatal issue for printing, especially for volumetric 3D scaffold architectures. To solve this problem, Habib et al. combined sodium alginate with carboxymethyl cellulose (CMC) to develop a novel hybrid hydrogel with good printability, shape fidelity, and cell viability, which showed as a potential biomaterial in the 3D bioprinting process [14]. Moreover, methylcellulose was used with low concentration of alginate (3%) for scaffold fabrication; the results showed good fidelity, improved gelation, and enhanced mechanical properties compared to pure alginate hydrogels [15]. In addition to improving their printability, the biological functionality of hydrogels could also be enhanced by integrating bioactive molecules, such as proteins and growth factors, into the scaffold. A novel multi-material hydrogel bioink composed of alginate, methylcellulose, and laponite nanoclay has been developed, and demonstrated good printability and cell viability [16]. Pelin et al. used low-cost plant-based cellulose microfibers in combination with gelatin and alginate without any prior modification to prepare a composite hydrogel-based 3D printer ink, which not only has the ability for printing a complex 3D porous structure, but also shows excellent cytocompatibility with fibroblast cells [17]. Moreover, Wang et al. designed a novel composite hydrogel material by adding hydroxyapatite nanoparticles into alginate/gelatin blends to fabricate bone scaffolds, which could promote osteogenic differentiation compared with pure alginate/gelatin scaffolds [18]. Chitosan (CS) is a natural cationic polymer obtained from the deacetylation of chitin, a renewable resource derived from crab and shrimp shells [19]. It has been widely used in tissue engineering due to its outstanding biocompatibility, biodegradability, non-antigenicity, and antibacterial activity [20, 21]. However, chitosan alone possesses poor printability and weak mechanical properties [22], and the stability of resulting structures can also be significantly diminished by swelling mechanisms in the aqueous environment [23]. Thus, chitosan-based multi-material hydrogels may overcome these challenges and increase the printability of chitosan-based blends. Gelatin, the denatured form of collagen protein, has been widely used to print tissue-engineering constructs as an optional supplement to enhance printability due to its reversible thermal-dynamic trait [24]. The solidification-yielding modulus and viscosity are significantly increased when the temperature of gelatin hydrogels drops [25] improved the printability and formability of such inks. Therefore, chitosan was incorporated into gelatin to tailor the printability and mechanical properties of scaffold for tissue engineering. Recently, Fischetti et al. blended chitosan and gelatin to establish a biocomposite ink for 3D printing scaffolds with improved shape retention [26]. Moreover, the biological functionality of scaffolds is a vital factor for the feasibility of hydrogel materials to support

cell attachment, differentiation, and vascularization. To this end, inspired by the development of chick embryos when many neo-vessels grow out of embryo and spread in the egg white transferring nutrition to the embryo, we surmised that egg white as an additive can increase the biological properties of hydrogel materials. Previous research has shown that egg white/alginate and egg white/alginate/gelatin hydrogel blends have great capacity for inducing vascularization within engineered tissues [27, 28]. Thus, in this work, a multi-material hybrid hydrogel made of chitosan, gelatin, and egg white, combining the advantages of each of the components, was explored for the fabrication of tissue-engineering scaffolds.

The mechanical strength and stability of the fabricated structures are vital factors for clinical application, and the crosslinking mechanisms are crucial in these aspects. In general, crosslinking techniques can be divided into chemical, physical, or enzymatic types [29]. Effective crosslinking strategies such as physical crosslinking alone are usually not efficient enough to fabricate mechanically stable scaffolds [30]. Therefore, designing or selecting an efficient crosslinking strategy is essential to construct a robust ready-to-use scaffold. Meanwhile, many crosslinking agents have been developed, which were mostly introduced to induce chemical interactions among accessible functional groups. Glutaraldehyde (GTA) and genipin (GP) are two of the most widely used crosslinking agents of collagen and gelatin due to their excellent crosslinking effect. Koc et al. employed GP to crosslink gelatin/chitosan-based hydrogels to investigate the swelling and drug release kinetics of the fabricated scaffold, and confirmed the suitability of such a combination [31]. Moreover, tripolyphosphate (TPP), as an alternative crosslinking agent, has been targeted due to its excellent biocompatibility [26]. Yu et al. presented the application of TPP to crosslink chitosan/gelatin blends developed for the growth of shape- and size-controlled calcium phosphates on/in these composites [32]. TPP, with multiple phosphate groups, interacts with the protonated amino groups of the macromolecular chains of chitosan. Thus, exploring a suitable crosslinking agent and the principles of chitosan/gelatin/egg white hybrid hydrogel is necessary for the construction of tissue-engineering scaffold with good fidelity, mechanical strength, and biocompatibility.

In view of the above, the aim of this work was to develop multi-material hybrid hydrogels with an optimal formulation of chitosan, gelatin, and egg white that can provide good printability, shape fidelity, and mechanical properties. Moreover, different crosslinking agents and principles based on GTA, GP, and TPP were evaluated and compared to select the optimum crosslinking strategy for this blend, in order to enhance the physicochemical and biological properties of the fabricated scaffolds.

Materials and methods

Materials

Chitosan (BR, 9012–76-4, 50–90 kDa, 80–95% deacetylation) was purchased from Sinopharm Chemical Reagent Co., Ltd (Shanghai, China). Gelatin (type A from porcine skin, 300 blooms) was obtained from Sigma-Aldrich (USA). Egg white (also called albumen) was isolated from chicken eggs obtained from a local supermarket (Shanghai, China). In brief, eggs were washed in deionized water and immersed into ethanol (75%) at room temperature (RT) for 30 min for surface disinfection. Then, the eggs were cracked, the egg white was separated from the yolk, and used in the preparation of composite hydrogels without further treatment. TPP, GP, and GTA as crosslinking agents were purchased from Sigma-Aldrich (Beijing, China).

Preparation of the chitosan/gelatin/egg white composite hydrogel

Firstly, as shown in Fig. 1a, chitosan powder was dissolved in 1% acetic acid (Sinopharm Chemical Reagent Co., Ltd) to produce 10% (w/v) chitosan solution. Gelatin was dissolved at a concentration of 18% (w/v) in deionized water at 60 °C using a tempered water bath. Then, chitosan–gelatin hydrogels (C–G) were prepared by mixing chitosan and gelatin solution in a 1:1 ratio. Finally, the prepared egg white was added to the C-G hydrogels at different volume ratios (E/C-G = 1:9, 2:8, 3:7, 4:6, and 5:5) to produce the egg white/chitosan/gelatin (E/C-G) composite hydrogels. All composite hydrogels were mixed thoroughly using a glass bar at room temperature to obtain homogeneous E/C-G blends.

Crosslinking strategies

In order to investigate the effect of different crosslinking agents on the properties of E/C-G composite scaffold, three different crosslinking agents were prepared according to the previous research: TPP and GP powders were dissolved in deionized water to prepare 15% (w/v) TPP [33] and 0.5% (w/v) GP [34, 35] aqueous solutions, respectively, and 0.25% (v/v) GTA [35, 36] aqueous solution was also prepared. These solutions were used to crosslink the printed scaffold, as shown in Figs. 1b–1d. Firstly, single crosslinking agents were used for crosslinking. In brief, the fabricated scaffolds were immersed into crosslinking solutions for 2 h and subsequently rinsed with phosphate-buffered saline (PBS). Secondly, a two-step crosslinking regime was established: TPP and GTA served as one group, whereas another group combined the crosslinkers TPP and GP. The fabricated scaffolds were separately immersed into the crosslinking solutions for 1 h each and finally washed with PBS.

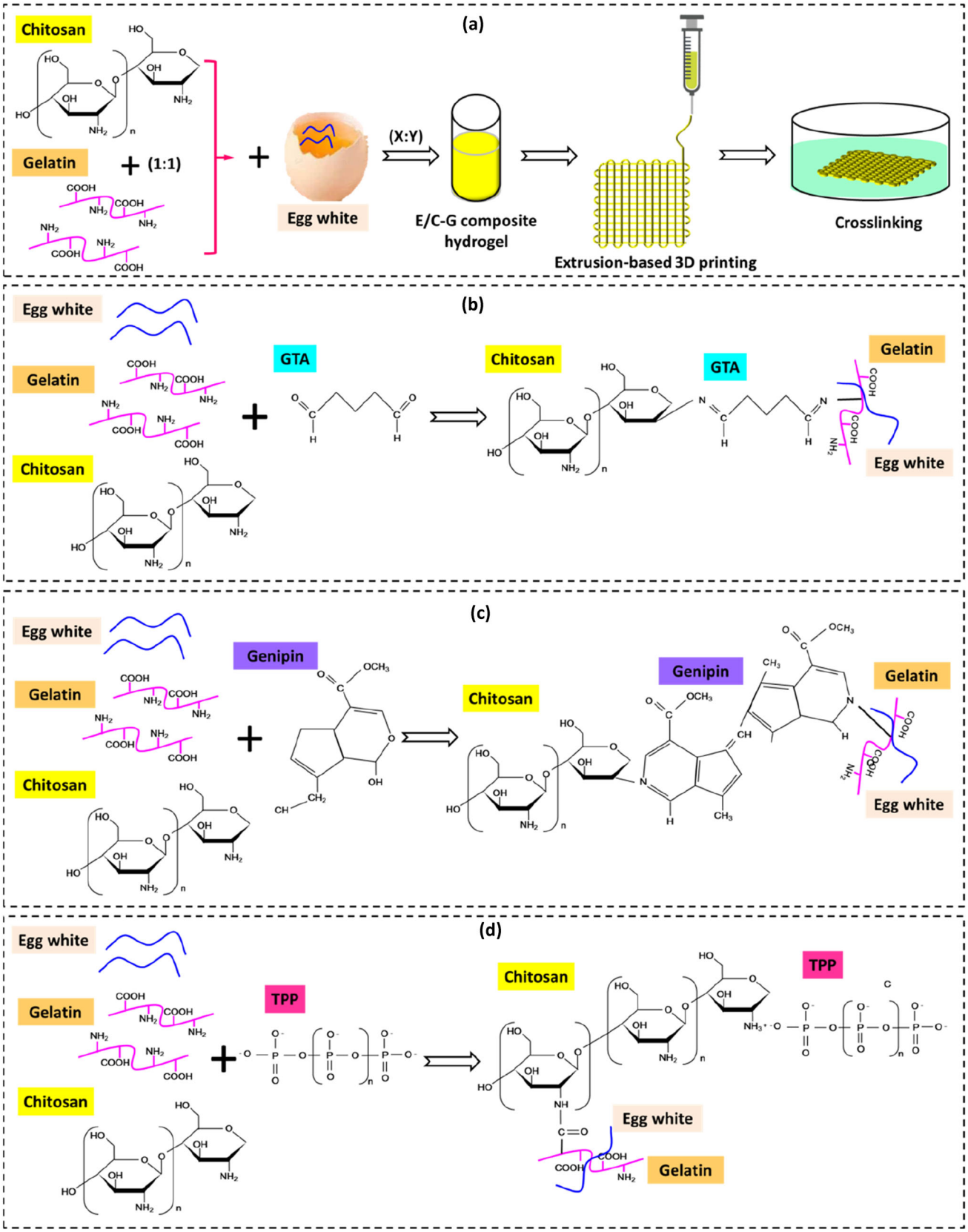

Fig. 1 **a** Schematic representation of the formulation and 3D printing of E/C-G composite hydrogel. **b**–**d** Schematic illustration of three crosslinking reactions studied for E/C-G composite scaffolds: **b** GTA crosslinking, **c** GP crosslinking, and **d** TPP crosslinking

Rheological testing of the E/C-G composite hydrogel

In order to analyze the printability of the E/C-G composite hydrogel, the rheological properties of the E/C-G blends with different volume ratios (E/C-G: 1:9, 2:8, 3:7, 4:6, 5:5) were tested by means of a rotational rheometer (DHR-3, Waters China Limited, China) with 25-mm-diameter plate geometry according to the manufacturer's protocol. All tests were conducted at a constant temperature of 25 °C under balanced conditions. The viscosity and shear-thinning behavior of E/C-G composite hydrogels was measured at constantly increasing shear rates from 0 to 300 s^{-1}. Moreover, the E/C-G composite hydrogels (volume ratio of 2:8) were crosslinked with the crosslinking strategies mentioned in Crosslinking strategies section along with the different crosslinking agents; the storage modulus and loss modulus of the crosslinked composite hydrogels were tested in a frequency range of 0.01–100 s^{-1}.

Printability assessment of the E/C-G composite scaffold

In order to evaluate printing fidelity, an extrusion-based 3D printing system (Rapid Manufacturing Engineering Center, Shanghai University) was implemented in this study. The main components of this printing system included an automated triaxial (*X*–*Y*–*Z*) stage along with the controller allowing a precision of 0.1 mm, a receiving platform, an air compressor (OTS-1100 × 2-60L 3P, Guangzhou Tiguan Trading Co., Ltd, China), a digital display pneumatic controller (TENSUN, Shenzhen, China), a medical syringe needle, a computer, and some air tubes. An air compressor was used to provide air pressure for extruding the materials; it was connected with the digital display pneumatic controller, and the syringe nozzle was linked to a digital display pneumatic controller by using the air tube for the convenience of controlling and displaying pressure. A G-code for a scaffold with a defined grid structure was written to form a 20 mm × 20 mm × 0.82 mm (L × W × H) cuboid structure, consisting of two layers with the adjacent layers perpendicularly stacked to ensure an open-porous structure. A Petri dish (100 mm, Corning, USA) was mounted to the receiving platform. The different E/C-G composite hydrogels described above were added to a medical syringe, and a 22G needle (internal diameter: 410 μm) was used for extrusion printing. The syringe was mounted in the *X*–*Y* plane of the automated triaxial stage. The air pressure value (65–350 kPa) to extrude the material was adjusted for each blend to generate a consistent filament and the best possible print. After printing, different crosslinking agents were poured into the Petri dish to immerse the entire scaffold in the respective solution for crosslinking according to Crosslinking strategies section. Images of the printed scaffolds before and after crosslinking were captured by a camera for the evaluation of printability of the different E/C-G composite hydrogels. The apparent evaluation criterion was as follows: the composite hydrogel was considered "printable" if it exhibited sufficient yield stress to prevent the collapse of the strands and ensured smooth extrusion out of the nozzle to form continuous filaments, such that no corrugation appeared (score = 1 means the best shape fidelity). If the extruded filament spread out after extrusion, this indicated that the material had insufficient yield stress to support its weight (score = 0.5 means medium shape fidelity). Contrarily, if the extrudate showed fractures within one filament, apparent "bead-like" structures along the filament, or problems to form a filament, it was considered as too brittle and non-printable (score = 0 means poor shape fidelity).

In addition, the printability of each E/C-G composite hydrogel was quantitatively assessed by measuring the strut size (filament diameter) along each filament and the formed pore area according to the previous literature [37]. Specifically, five points were randomly chosen along each filament where the strut size across that point was measured. The formed pore area of adjacent fibers was also tested (at least five pores were tested). Then, the pore area error and the strut size error were introduced to quantify the fidelity of filaments, which are defined by the following formula:

$$\text{Strut size error } (\%) = \frac{S_t - S_d}{S_d} \times 100\%,$$

$$\text{Pore area error } (\%) = \frac{|P_t - P_d|}{P_d} \times 100\%,$$

where S_t represents the tested average strut size value of fibers, S_d represents the designed size (equal to the inner diameter of nozzle: 0.41 mm), P_t represents the measured average pore area, and P_d represents the designed pore area (6.76 mm^2).

In order to further test the supportability of extruded fibers, a filament collapse test was conducted according to a previous research [14]. The mid-span deflection of a suspended filament was evaluated to determine the composite hydrogel collapse. A platform was designed by CAD software SolidWorks 2018, which consisted of seven pillars with known spaces of 1, 2, 3, 4, 5, 6 mm, respectively, as will be shown in Figs. 3h and 3j. The width of each pillar was 2 mm, and the platform was fabricated by using a fused deposition modeling (FDM) printer with PLA material, as will be shown in Fig. 3i. 22G nozzles (internal diameter: 0.41 mm) were used, and a constant printing pressure (180 kPa) and speed (5 mm/s) were applied. A single filament of different E/C-G hydrogels was deposited on this platform, as will be shown in Fig. 3k. The angle between the collapse and the horizontal plane (as will be shown in Fig. 3k) was measured to quantify the supportability of fibers with different ratios; for visualization, a red dye was added.

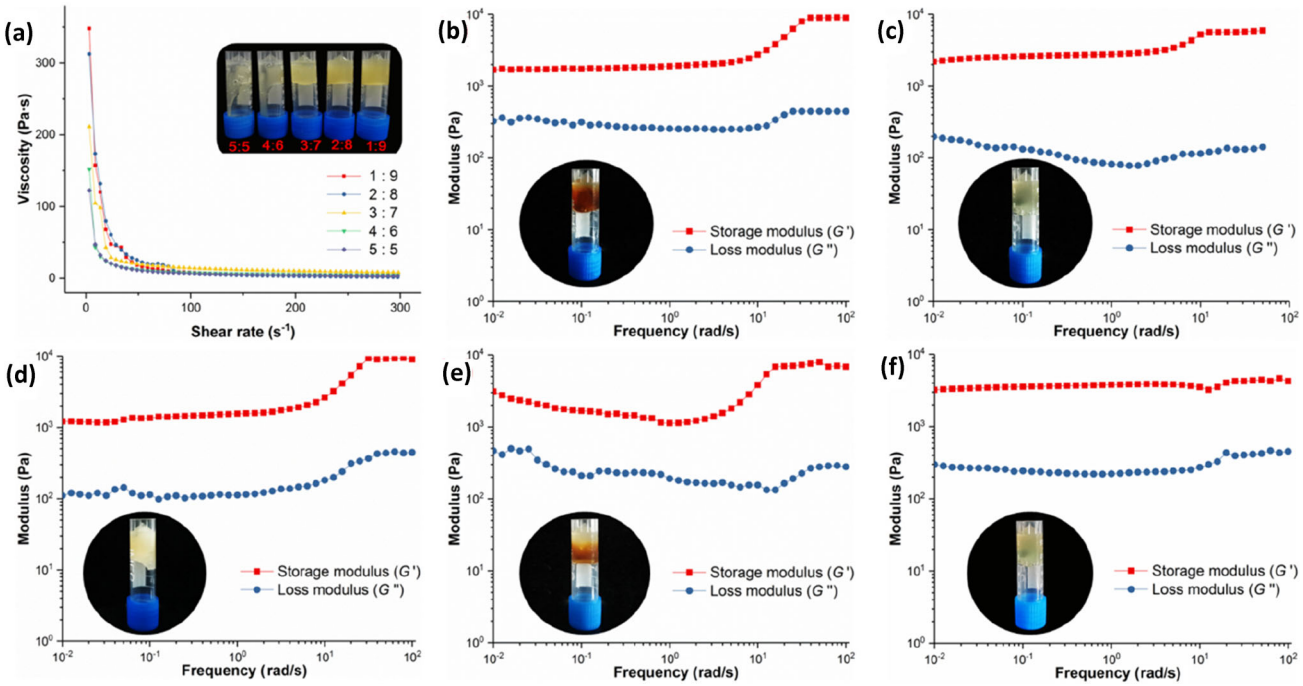

Fig. 2 Flowability and rheological properties of the prepared E/C-G composite hydrogels. **a** The flowability and viscosity of the hydrogels (shear ramp 0–300 s^{-1}): all of the E/C-G composite hydrogels with different volume ratios exhibited strong shear-thinning behavior; **b–f** the storage (G') and loss (G'') modulus of the E/C-G hydrogels after being crosslinked using different agents and methods: **b** GTA, **c** GP, **d** TPP, **e** TPP + GTA, **f** TPP + GP

In order to study the effect of different crosslinking agents on the filament size, composite hydrogel filaments (E/C-G = 2:8) were printed, and the diameter of filaments was measured before crosslinking (D_1). Then, the filaments were immersed into different crosslinking solutions according to Crosslinking strategies section. The diameter of the filaments after crosslinking was determined (D_2). We introduced the crosslinking shrinkage ratio to quantify the effect of different crosslinking strategies on the filament size, which is defined by the following formula:

$$\text{Crosslinking shrinkage ratio } (\%) = \frac{D_1 - D_2}{D_2} \times 100\%.$$

Porosity measurement of the E/C-G composite scaffold

The porosity of the fabricated E/C-G composite scaffold (E/C-G = 2:8) with different crosslinking treatments was measured by the gravity bottle method, as introduced previously [38, 39]. In brief, a vacuum freeze dryer (LGJ-10D, Beijing Science Instrument, China) was used to dry the specimens, and ethanol was used as the testing liquid because it permeated through the scaffolds without inducing matrix swelling or shrinkage. The porosity ratio of the specimens was calculated by the following formula:

$$\text{Porosity ratio } (\%) = \frac{W_1 - W_3 - W_d}{W_2 - W_3} \times 100\%,$$

where W_d represents the weight of the dried specimens, W_1 represents the weight of the specimens immersed into the specific gravity bottle filled with ethanol, W_2 represents the weight of a specific gravity bottle filled with ethanol, and W_3 represents the weight of the specific gravity bottle filled with ethanol after removing the specimens.

Crosslinking degree

The crosslinking degree of the fabricated E/C-G composite scaffolds with different crosslinking treatments was assessed by the ninhydrin test to determine the content of free amino groups according to previous protocols [35, 40]. Briefly, a ninhydrin solution kit (purchased from Wako, Japan) was utilized. The fabricated crosslinked and uncrosslinked scaffolds were weighed and heated in 10-mL ninhydrin solution at 80 °C for 15 min. Then, the container was removed to cool for 15 min at room temperature, and the absorbance of the solutions (C) was measured by a UV–Vis spectrophotometer (Evolution™ 350, Thermo Scientific) at 570 nm using glycine at various known concentrations as the standard. The

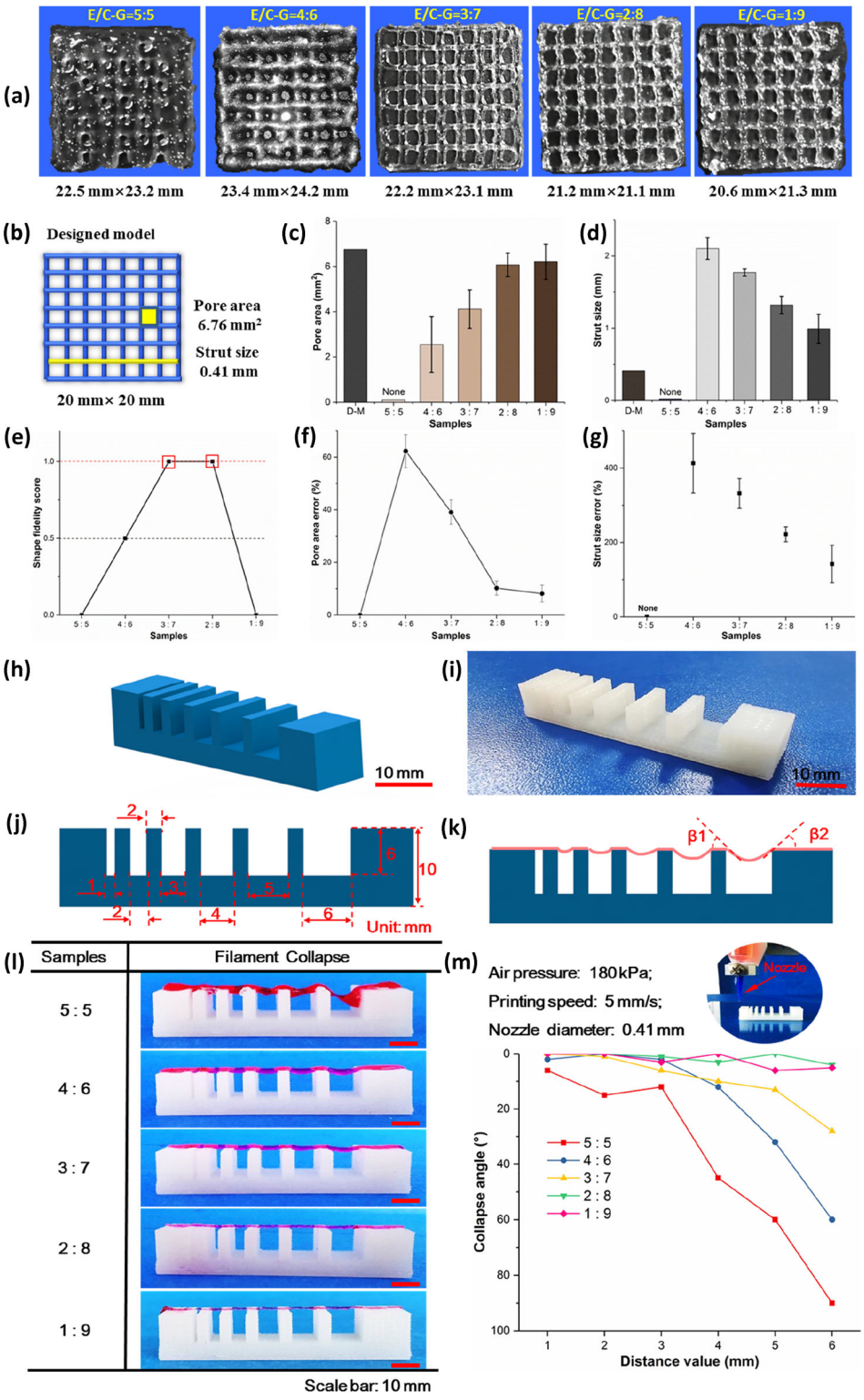

Fig. 3 Shape fidelity and printability of the prepared E/C-G composite hydrogels with different volume ratios (E/C-G = 1:9, 2:8, 3:7, 4:6, and 5:5). **a** macrographs of the printed E/C-G composite scaffolds with different ratios, and the dimension of the structures; **b–g** quantitative analysis of the shape fidelity: **b** designed model of the printed scaffolds, **c** pore area of printed E/C-G composite scaffolds, **d** strut size of printed E/C-G composite scaffolds, **e** shape fidelity scores of different E/C-G composite hydrogels according to the evaluation criteria of the printed structures (shown in (**a**)), **f** pore area error corresponding to (**c**), **g** strut size error corresponding to (**d**); **h–m** filament collapse test: **h** the designed testing platform, **i** FDM-printed testing platform consisting of PLA, **j** the designed dimension of the testing platform, **k** determination of collapse angle, **l** photographs showing the filament collapse appearance (red) of different E/C-G composite hydrogels, **m** collapse angles at different distances for different E/C-G composite hydrogels (the error bars represent the standard deviation; $n = 3$)

crosslinking degree for each scaffold was calculated as follows:

$$\text{Crosslinking degree } (\%) = \left(1 - \frac{C_{\text{crosslinked}}}{C_{\text{uncrosslinked}}}\right) \times 100\%.$$

Effect of crosslinking technique on the mechanical properties of E/C-G composite scaffolds

A WDW-1 materials testing machine (Songdun Machine Equipment Co., Ltd, Shanghai, China) was used to test

the tensile mechanical properties of the E/C-G composite scaffold. The printed E/C-G composite scaffolds were crosslinked by different crosslinking principles mentioned in Crosslinking strategies section as the testing specimens. The testing specimens were mounted and stretched in the vertical direction at a strain rate of 0.5 mm/min at RT. The stress–strain curves were captured, and the maximum tensile strength and Young's modulus were recorded. Three specimens in each group were subjected to the testing protocol.

Effect of different crosslinking processes on the surface hydrophilicity of E/C-G composite scaffolds

In order to evaluate the effect of different crosslinking principles on the wettability of E/C-G composite scaffold, an optical contact angle meter (OCA 15EC, EASTERN-DATAPHY, China) was used to examine the static water contact angle at room temperature through the sessile drop method. Specifically, 20 μL of water droplets were formed on a needle and dropped onto the surface of the tested specimens. The images of the contact angle were obtained, and auto-analysis was performed by drop shape analysis. The contact angle was measured as the tangent to the interface of the droplets on the specimens. The surface hydrophilicity of the cross section of crosslinked bulk was also measured. At least, three test runs were taken for each specimen, and the averaged values were calculated.

Effect of different crosslinking methods on the swelling property of E/C-G composite scaffold

In order to assess the effect of different crosslinking agents on the swelling properties, after the application of different crosslinking processes as described in Section "Crosslinking strategies", the E/C-G composite scaffolds were separately immersed in phosphate buffered saline (PBS, pH 7.4) and DME/F-12 cell culture medium at 37 °C for 2 h. The weight of the swollen scaffolds (W_s) was defined after removing excess water from the surface. The dry weight (W_d) of the scaffolds (dried using a drying oven at 37 °C) was measured, and the swelling ratio was calculated according to the following equation:

$$\text{Swelling ratio } (\%) = ((W_s - W_d)/W_d) \times 100\%.$$

The swelling ratio of filaments is another vital parameter impacting the printing fidelity of scaffolds. The dimensional change in each of the printed E/C-G composite filaments was measured using a microscope every 10 min until no obvious further change was recorded. The swelling ratio of filaments was calculated according to the formula $(D_t - D_o)/D_o \times 100\%$, where D_t and D_o represent the value of dimensional swelling at different time points and the initial dimension prior to soaking, respectively.

Degradation rate

In order to evaluate the effect of different crosslinking principles on the degradation of E/C-G composite scaffolds (10 mm × 10 mm × 0.82 mm), the in vitro degradation was tested in PBS (pH 7.4) and DME/F-12 medium at 37 °C. Briefly, the crosslinked scaffold was placed into a drying oven at 37 °C, and the dry weight of the scaffold was recorded as W_o. Next, the scaffold was immersed into a testing container with PBS or cell culture medium (5–6 mL volume, making sure that the scaffold was fully immersed) and steeped for 30 days. The dry weight of the scaffold after the given number of days was recorded as W_t. The percentage of degradation ratio of the scaffold was calculated as follows:

$$\text{Degradation ratio } (\%) = \frac{W_t - W_o}{W_o} \times 100\%.$$

Preparation of cell seeding experiments

Human umbilical vein endothelial cells (HUVECs, The Second Military Medical University, China) were routinely cultured in DME/F-12 (1:1) medium supplemented with 10% fetal bovine serum and 1% penicillin/streptomycin. The cells were resuscitated and cultured in a standard Petri dish (Corning, USA) in a humidified incubator with 5% CO_2 at 37 °C. The culture medium was refreshed every day, and cells were passaged at 80% confluency using Trypsin–EDTA (0.25%) with phenol red. A final cell suspension density of 1×10^6 cells/mL was used for the subsequent seeding experiments.

Biological characterization of the crosslinked E/C-G composite scaffold

In order to evaluate the cytocompatibility and potential cytotoxicity of the crosslinked E/C-G composite scaffolds, they were seeded with HUVECs. In brief, the prepared E/C-G composite scaffolds were immersed into 75% ethanol for 6 h under UV light radiation, and the samples were flipped after 3 h. Then, the scaffolds were removed and washed with PBS three times. Finally, the composite scaffolds were immersed into freshly prepared medium under UV light for 2 h before inoculation. The prepared cell suspension (1×10^6 cells/mL, 200 μL) was gently poured onto the surface of the scaffolds until they were fully covered, which were then placed into a humidified incubator for 4 h to allow adherence. Following adhesion, 3 mL of freshly prepared medium was added into the dish until the upper surface of the scaffold was covered;

seeded samples were moved into the incubator for cultivation at 37 °C in 5% CO_2, with the culture medium refreshed every day thereafter.

A live/dead cell staining kit (Yeasen, Shanghai, China) was employed to assess the viability of cells on the scaffolds after cultivation for 2 and 4 days. All operations were carried out according to the manufacturer's protocol. Briefly, the staining solution was prepared by mixing 1 μL of Live-Dye (Calcein-AM) and 3 μL Dead-Dye (PI solution) into 1 mL of assay buffer. After culturing for 2 and 4 days, the cell-seeded E/C-G composite scaffold was removed from the culture medium and placed into a new dish to rinse with PBS. Then, the prepared staining solution was evenly dripped onto the scaffold surface, which was then incubated for 15 min at 37 °C. Finally, the redundant staining solution was washed away using PBS, and the scaffold was mounted on microscope slides for observation using an inverse fluorescence microscope (Eclipse Ti–U, Nikon Instruments Inc., Japan). The cell viability on the prepared scaffolds treated with different crosslinking methods was calculated, and the cell images of the scaffold were captured after culturing 4 h, 2 days, and 4 days; also, the coverage rate of live cells on the scaffolds was quantified by using ImageJ software (NIH Image). Moreover, to further visualize the cell morphology, the cell nuclei and cytoskeleton were stained with 4',6-diamidino-2-phenylindole (DAPI) and tetramethylrhodamine (TRITC) phalloidin, respectively. In brief, after 4 days of culture, the cell-seeded scaffolds were rinsed with PBS, fixed with 4% paraformaldehyde, and permeabilized with 0.5% Triton X-100; TRITC − phalloidin was used to stain the cell cytoskeleton in a dark environment for 30 min, and DAPI solution was applied for 30 s to stain the cell nucleus. Subsequently, the fluorescence images were captured.

In addition, the morphology of the attached cells in the scaffold was examined by scanning electron microscopy (SEM). As a preparation for this procedure, the crosslinked scaffolds with TPP and TPP + GP were tested after cultivation for 2 and 4 days. The seeded scaffolds were fixed with 2.5% glutaraldehyde (Sigma) for 24 h at room temperature. After gentle washing three times with PBS, the fixed cell-seeded scaffolds were dehydrated in a series of graded ethanol (25%, 50%, 75%, 85%, 95%, and 100%) for 5 min each. Then, the scaffolds were immersed into the mixed solutions of absolute ethanol and hexamethyl disilylamine (3:1, 1:1, 1:3, and 0:1) for 10 min each to remove the alcohol, followed by sputter coating with gold before imaging. The obtained SEM images were evaluated by using ImageJ software (NIH Image) for a semi-quantitative analysis of cell proliferation, and the coverage ratio of adherent cells on the surface of the scaffold was calculated by using the following equation as described in a previous study [41]:

$$\text{Coverage ratio } (\%) = (S_a/S) \times 100\%,$$

where S_a represents the covered area of cells attached to the surface of the scaffold in the SEM image, and S represents the total area of the surface of the scaffold in the SEM image.

Cell proliferation assay

In order to analyze the effects of different crosslinking methods for the fabrication of E/C-G composite scaffolds on cell proliferation, a cell counting kit (CCK-8, KeyGEN BioTECH, Shanghai, China) was used to test cell proliferation on day 0, 2 and 4 of the experiment according to the manufacturer's protocol, as described previously [42]. In short, the E/C-G composite scaffolds were sterilized and washed with PBS. Then, the scaffolds were cut into small pieces (6 mm × 6 mm × 0.82 mm) using sterilized surgical scissors, and immersed into fresh culture medium for 2 h under UV light. Pieces of scaffold and cell suspension at a concentration of 2×10^5 cells/mL were seeded into 24-well plates (No. 3524; Costar) at 1 mL of suspension and one piece of scaffold per well. The E/C-G composite scaffolds fabricated with different crosslinking principles according to Section "Crosslinking strategies" were tested. Moreover, the freshly prepared medium and cells were seeded into other wells of 24-well plates in 2D without a scaffold as the control group. One row of wells of each plate acted as a background group, only containing the culture medium. After seeding, the plates were incubated in a CO_2 incubator at 37 °C. At different time points determined in the experimental design, 0.1 mL CCK-8 reagent was added into each well and incubated for 2 h at 37 °C. The absorbance of each well was measured to evaluate the metabolic activity of cells by using a microplate reader (Infinite 200 PRO, Tecan Group Ltd., Switzerland) at a wavelength of 450 nm after culturing for 0, 2, and 4 days. The data of day 0 refers to the adhesion 4 h after seeding. Each testing sample consisted of at least six wells.

Assessment of in vivo angiogenic potential using a chick embryo model

In order to test our original hypothesis, the angiogenic potential of the prepared E/C-G composite scaffold (TPP crosslinking only) was evaluated. The chick embryo chorioallantoic membrane (CAM) assay was used for this purpose, with the quantitatively analysis of neo-vessel formation. In brief, fertilized chick eggs were incubated horizontally at 37.8 °C in a humidified atmosphere, with the beginning of incubation referred to as embryonic day 0. After incubation for 4 days, a circular window was opened in the air chamber between the CAM and the egg shell. This window was sealed with transparent adhesive tape, and the eggs were returned

to the incubator. On day 7, a 10 mm × 10 mm sterile E/C-G composite scaffold was implanted on top of the CAM; meanwhile, a 10 mm × 10 mm sterile C-G composite scaffold (TPP crosslinking only) was set as the control group. The eggs were re-sealed and returned to the incubator for 7 days, and were humidified every day. On day 14, the transparent adhesive tape was removed, and the morphology of scaffolds was imaged by a camera. Then, embryos were euthanized by adding a fixative (2 mL) on top of the CAM. Then, the CAM with the implanted scaffold was harvested and immediately fixed in 10% buffered formaldehyde. Meanwhile, the inoculation area of the CAM with the implanted scaffold was photographed by a digital camera (Mi 11, Xiaomi, China). All of the operation instructions and inoculation processes were presented (as will be shown in Fig. 9a).

For the quantitative analysis of the total number of neovessels, the images of the inoculation area of the CAM with the implanted scaffold were analyzed using ImageJ according to a previous study [43] using the "Ridge (Line) Detection Plugin," and including the control group. Moreover, the fixed CAM with the implanted scaffold was dehydrated, embedded in paraffin and cut into 5-μm-thick sections with a microtome. The sections were stained with hematoxylin–eosin (HE) and Masson stain following the manufacturer's instructions.

Statistical analyses

All results were expressed as mean ± standard deviation (SD). Statistical analysis was performed by single-factor analysis of variance (ANOVA) with Tukey's post hoc test, and the value of $p \leq 0.05$ was considered statistically significant. Origin 2017 software was used.

Results and discussion

Preparation and characterization of the E/C-G composite hydrogel

Biomaterials play a crucial role in 3D printing applications for biomedical tissue engineering, especially multi-material composite hydrogels, which, combined with the individual advantages of different materials, can provide an inhabitable temporary environment for cells to adhere, proliferate, and differentiate into a specific tissue lineage. In this work, a series of novel E/C-G composite hydrogels with varying composition (C/G = 1:1; E/C-G = 1:9, 2:8, 3:7, 4:6, and 5:5) were developed by mixing chitosan, gelatin, and egg white according to Section "Preparation of the chitosan/gelatin/egg white composite hydrogel". The flowability of the E/C-G composite hydrogel with different volume ratios could be observed in cryogenic vials (Fig. 2a), indicating that a 3:7 volume ratio of E/C-G can be considered as the transition point from under- to over-gelation. Before this point (i.e., 4:6 and 5:5), the E/C-G composite hydrogels have high fluidity, i.e., low viscosity. Inversely, the flowability of the E/C-G composite hydrogel decreases with the decrease in egg white content. Compared to our previous research [27, 44], herein, the high flowability (i.e., low viscosity) of biomaterials resulted in poor printability and insufficient shape fidelity of the printed scaffold by deliquescing after extrusion.

The rheological behavior of the bioink plays a crucial role in its printability. In particular, biomaterials with appropriate viscoelastic properties contribute to the bioprinting of tissue-engineering scaffolds that can carry cells and therapeutic molecules/drugs. The viscoelastic properties of the fabricated E/C-G composite hydrogels with different volume ratios exhibited shear-thinning behavior (Fig. 2a). The decrease in viscosity with the increase in shear rate (i.e., shear-thinning response) is a typical behavior of non-Newtonian fluids [45], and an essential requirement for extrusion printing. This characteristic is similar to that of previously developed bioinks [9, 46, 47] that promote the viability of entrapped cells due to the alleviated shear stress when passing through the printing nozzles at a certain flow rate. It is known that for the extrusion-based 3D printing of chitosan-based blends and other hydrogels [22, 26], the shear-thinning behavior of the material is a prerequisite [48]. Moreover, crosslinking reactions have been commonly used in the fabrication process of tissue-engineering scaffolds to speed up the gelation and further increase their mechanical strength and hydrolysis resistance in in vitro/vivo culture [49]. To verify the availability of different crosslinking mechanisms on the E/C-G composite hydrogel, we tested the storage modulus and loss modulus of the crosslinked composite hydrogels (2:8) after applying different crosslinking processes according to Section "Rheological testing of the E/C-G composite hydrogel" (Figs. 2b–2f). The shear stress sweep graphs show a higher storage modulus and a lower loss modulus of the crosslinked composite hydrogel according to the applied crosslinking agents. This further evidences that the prepared E/C-G composite material can be crosslinked to form a stable gel and have the ability to retain its shape, thus it has great potential for the 3D printing of tissue-engineering scaffolds.

Printability assessment of the E/C-G composite scaffold

The development of extrusion-based 3D printing for tissue engineering is conditioned by the design and preparation of biomaterials with adequate printability and shape stability. To evaluate these properties of the prepared E/C-G composite hydrogel, the E/C-G hydrogel precursors with different ratios

were used to print a grid structure (L × W × H = 20 mm × 20 mm × 0.82 mm) using a self-developed extrusion-based 3D printing system. Photographs of the printed structure (Fig. 3a) were taken, and the actual side length was measured. (The corresponding measurements are shown in Fig. 3a). To further quantify the accuracy of the scaffold, images were used to measure the pore area and the strut size by ImageJ, and the results are summarized in Figs. 3c and 3d. By comparing these to the theoretical values of the original design model (Fig. 3b), the respective errors for the pore size and the strut size were calculated (Figs. 3f and 3g). Furthermore, a shape fidelity score (Fig. 3e) was assigned according to the morphological characteristics of the printed structure, which is introduced in Section "Printability assessment of the E/C-G composite scaffold". The 5:5 hydrogel sample possessed no shape fidelity and immediately lost its structure after being printed (Fig. 3a), resulting in a puddle (Fig. 3e); hence, the pore area and strut size could not be measured (Figs. 3c and 3d), and the score was defined as 0. The 4:6 hydrogel samples, where the designed structure was still maintained and visible after printing, performed better than the 5:5 samples. However, the filaments exhibited excessive softness and expansion after extrusion (Fig. 3a); hence, the fidelity of scaffold was evaluated as rather poor (score = 0.5). From the 3:7 and 2:8 hydrogel groups, both scaffolds with clear and defined edges could be printed, while the 3:7 group deliquesced within a few minutes after printing. However, both groups showed good shape fidelity (score = 1) according to the evaluation criteria of the printed structure. Although the 1:9 hydrogel group could maintain the structure that imitated the designed model, the extruded filament showed fractures and unevenness, resulting in irregular and fragmentary scaffolds; thus, this group was considered as too brittle and exhibiting poor shape fidelity (score = 0). In terms of quantitative analysis, the pore area of all printed structures appeared to present a trend of increasing pore area with reduced egg white concentration, ranging from 2.55 ± 1.23 (4:6 group) to 6.21 ± 0.78 mm^2 (1:9 group), as shown in Fig. 3c. This trend was less drastic when comparing the 2:8 group (6.07 ± 0.52 mm^2) to the 1:9 group (6.21 ± 0.78 mm^2), with values close to the pore area of the designed model (6.76 mm^2, Fig. 3b). For the extruded strut size, there seemed to be a general trend of decreased strut size with the decrease in egg white concentration, ranging from 2.02 ± 0.15 (4:6 group) to 0.99 ± 0.2 mm (1:9 group), as shown in Fig. 3d. However, all values of strut size were higher than the value of the designed model, which was caused by the extrusion expansion effect [14]. Moreover, through the quantitative analysis of the pore area and strut size errors, the percentage of all errors decreased with the reduction in egg white concentration (Figs. 3f and 3g). The minimum pore area error was found in the 1:9 group ((8.1 ± 3.2)%), whereas the value of the 2:8 group was (10.2 ± 3.2)%. Similarly, the minimum strut size was observed in the 1:9 group, with the value of (142.1 ± 51.1)% (i.e., 1.42-fold compared to the inner diameter of the nozzle). The value of the 2:8 group was (221.5 ± 22.1)% (i.e., 2.21-fold).

In addition, filament collapse tests were conducted to further determine the supportability of the E/C-G hydrogels. The qualitative observation of the collapse test for various volume ratios of E/C-G hydrogels showed that decreasing concentrations of egg white led to less deflection of the printed filaments, as shown in Fig. 3l. The 2:8 and 1:9 hydrogels generated a nearly straight filament without collapse on the pillars situated at various distances (max. 6 mm). The angles between the collapse and the horizontal plane for each distance value of each material composition were measured according to the protocol described in Section "Printability assessment of the E/C-G composite scaffold". The angles of each filament showed an increasing trend with the increase in pillar-to-pillar distance (Fig. 3m). The graph indicates that the 5:5 group was not able to maintain the filament geometry and obviously collapsed at 4 mm and larger distances. Although the 4:6 and 3:7 groups could maintain the integrity of the filament, the obviously concave shape appeared at 4 mm distance, and it worsened with the further increase in distance. The 2:8 and 1:9 groups showed minimum angles between the collapse and the horizontal plane even with the increase in distance. However, the filament diameter of the 1:9 group was thinner than that of the 2:8 group, which might be caused by the extrusion content due to the viscosity difference. Moreover, composite hydrogel scaffolds with different thickness were printed by using 2:8 E/C-G hydrogel, namely, two-layered structure: 20 mm × 20 mm × 0.82 mm, four-layered structure: 20 mm × 20 mm × 1.64 mm, six-layered structure: 20 mm × 20 mm × 2.46 mm, and eight-layered structure: 20 mm × 20 mm × 3.28 mm (L × W × H), as shown in Fig. 4a. Even in large dimensions, an open macroporous structure could be maintained, which is crucial for cell viability as it ensures oxygen and nutrient supply throughout the scaffold [42, 48]. Based on the above, through the comprehensive evaluation of the print characteristics of all E/C-G hydrogel precursors with different ratios, the 2:8 E/C-G composite hydrogel exhibited good printability and shape fidelity for the designed 3D printing process of tissue-engineering scaffold fabrication. Therefore, this E/C-G ratio (2:8) was selected for the further experiments described below.

Effect of different crosslinking methods on the properties of E/C-G composite scaffold

Scaffold morphology and shrinkage ratio

The macroscopic morphology of the crosslinked E/C-G composite scaffolds after treatment with different crosslinking reagents was captured, which revealed different colors of the scaffolds, as shown in Fig. 4b. The non-crosslinked E/C-G

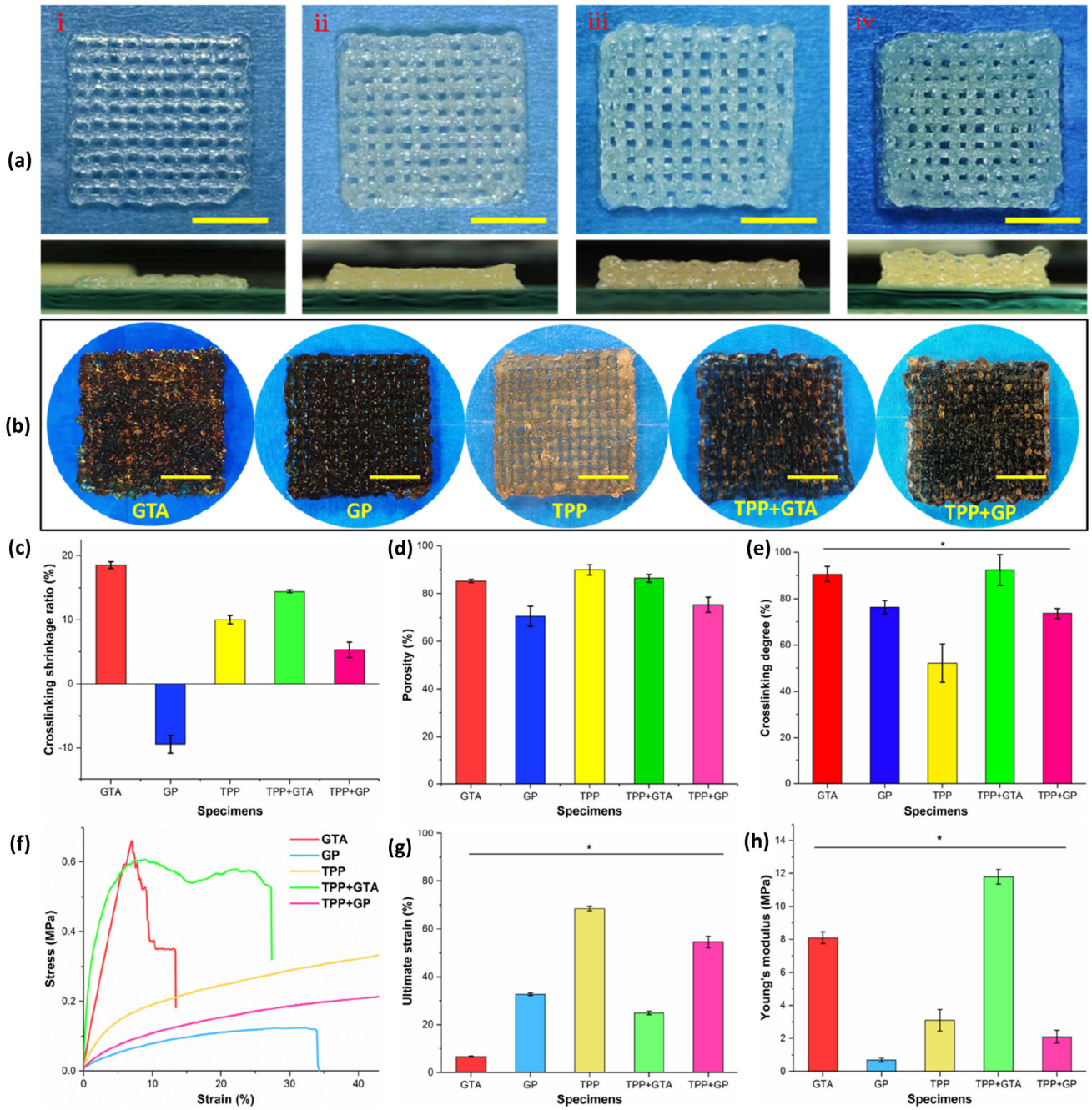

Fig. 4 **a** The 3D-printed E/C-G (2:8) composite scaffolds (non-crosslinked) with different thicknesses: (i) two-layered structure: 20 mm × 20 mm × 0.82 mm (L × W × H); (ii) four-layered structure: 20 mm × 20 mm × 1.64 mm (L × W × H); (iii) six-layered structure: 20 mm × 20 mm × 2.46 mm (L × W × H); (iv) eight-layered structure: 20 mm × 20 mm × 3.28 mm (L × W × H), scale bar: 10 mm; **b** Appearance of the crosslinked E/C-G (2:8) composite scaffolds fabricated through different crosslinking methods, scale bar: 10 mm; **c** shrinkage ratio of the printed filament size; **d** porosity, **e** crosslinking degree, and **f**–**h** mechanical properties (**f**: representative stress–strain curves, **g**: ultimate strain, **h**: Young's modulus) of the differently crosslinked E/C-G composite scaffolds. The error bars represent the standard deviation ($n = 3$) and a value of $^{*}p \leq 0.05$ was considered statistically significant

composite hydrogel exhibited a pale yellow coloration. The printed E/C-G composite scaffold crosslinked by GTA was deep yellow and GP-crosslinked scaffolds were greenish-blue, while the color of the TPP-crosslinked scaffold was similar to the non-crosslinked E/C-G hydrogel, presenting a translucent pale yellow color. The color of the TPP + GTA-crosslinked scaffold was similar to the GTA-crosslinked scaffold, which could be caused by the dominant color of the crosslinking product formed with GTA. The TPP + GP-crosslinked scaffold showed the alternating colors of deep

blue and pale yellow, which might be affected by the short GP crosslinking time (1 h). We inferred that the TPP + GP-crosslinked scaffold would also present a greenish-blue color with longer GP crosslinking time (2 h), similar to scaffolds crosslinked with GP only. The shrinkage ratio of crosslinked filament size, a key parameter to evaluate the fidelity of the prepared scaffolds, was measured after application of the different crosslinkers, with the results shown in Fig. 4c. The shrinkage ratio of GTA-crosslinked filament was (18.5 ± 0.5)%, that of the TPP-crosslinked filaments was (10.2 ± 0.6)%, that of the TPP + GTA group was (14.4 ± 0.5)%, and that of the TPP + GP group was (5.3 ± 1.2)%, while that of the GP-crosslinked filament was (− 9.4 ± 1.4)%. We found that the diameter of the filaments enlarged after GP crosslinking, which might be caused by the low GP concentration of the applied solution and the short crosslinking time. The shrinkage ratio of GTA-crosslinked filament was the largest among all, indicating that GTA had the best crosslinking efficiency. However, the comparison of the filament size of scaffold before and after crosslinking revealed that the slight shrinkage of all scaffolds had no significant impact on the feature resolution of the printed scaffold.

Porosity and crosslinking degree

Porosity is considered an essential parameter of scaffolds for tissue engineering and regenerative medicine, as it greatly influences the cell penetration and mass transport of oxygen, nutrients, and overall metabolism [50]. The porosity of the E/C-G composite scaffolds (E/C-G: 2:8) treated with different crosslinkers was separately measured (Fig. 4d). The porosity of the GTA-crosslinked scaffold was (84.3 ± 0.65)%; the GP-crosslinked scaffold showed lower porosity ((70.5 ± 4.2)%) than the GTA group; the porosity of the TPP-crosslinked scaffolds was (88.3 ± 2.2)%, the largest among all groups; the porosity of TPP + GTA- and TPP + GP-crosslinked scaffolds was (85.5 ± 1.65)% and (75.3 ± 3.1)%, respectively. All of the scaffolds crosslinked with different reagents showed adequate porosity (> 65%) and therefore were considered suitable for cell colonization and infiltration [35]. The porosity of scaffolds with dual crosslinking (TPP + GTA, TPP + GP) was not significantly different compared to that of scaffolds with single crosslinking groups (GTA, GP, and TPP). To further quantify the effect of different crosslinking regimes on E/C-G composite scaffold, the crosslinking degree of scaffold was determined by the ninhydrin protocol through measuring the content of free amino groups. The results illustrated in Fig. 4e showed that the crosslinking degree of E/C-G composite scaffold crosslinked with GTA, GP, TPP, TPP + GTA, and TPP + GP was (90.65 ± 3.12)%, (76.35 ± 2.86)%, (52.22 ± 8.23)%, (92.38 ± 6.65)%, and (73.67 ± 2.12)%, respectively. The crosslinking degree of E/C-G composite scaffold treated with TPP + GTA was higher than that of the other groups. Inversely, the E/C-G composite scaffold crosslinked with TPP had the lowest crosslinking degree. Many previous studies [21, 23, 31, 35] have reported the commonly used crosslinking agents for chitosan-based hydrogel scaffolds as GTA, GP, and TPP. To the best of our knowledge, the different crosslinking methods (GTA, GP, TPP, TPP + GTA, and TPP + GP) have not yet been comparatively studied for E/C-G composite hydrogel scaffold for tissue engineering. The results showed that the GTA and TPP + GTA provided excellent crosslinking effects, which testified the good crosslinking property of GTA. However, GTA has been widely reported as cytotoxic, which limits its applicability for medical purposes [51, 52]. There is thus a concern with GTA residues in the crosslinked hydrogels, and inactivating the aldehyde groups of the residue GTA with glycine or rinsing with abundant water/PBS has been reported [53]. The crosslinking degree of GP, TPP, and TPP + GP was lower than that of the other two groups, and the degree of crosslinking with GP was higher than that of TPP. GP, which is known to possess high biocompatibility, is a naturally occurring crosslinking agent [23]; however, it is fairly expensive. As for the TPP crosslinking agent with its multiple phosphate groups, a previous study reported that it is able to interact with the protonated amino group of chitosan [21]. Tripolyphosphate has received increasing attention as an alternative crosslinking agent due to its excellent biocompatibility and low price.

Mechanical properties

The mechanical properties of scaffolds constitute a very important parameter in many tissue-engineering applications. The representative tensile stress–strain curves of scaffolds crosslinked using different methods in our study are shown in Fig. 4f, and the ultimate strain is recorded as in Fig. 4g. Meanwhile, the Young's modulus of these scaffolds was calculated from the stress–strain curves, and the values are shown in Fig. 4h. The tensile strength of GTA-crosslinked scaffold (0.66 ± 0.02 MPa) was higher than that of the other groups; inversely, the GTA-crosslinked scaffold showed the lowest strain ((6.94 ± 0.15)%). The TPP + GTA-crosslinked scaffold also exhibited excellent mechanical strength (0.60 ± 0.05 MPa), and the tensile strain of this group was larger than that of the GTA group but much lower than that of the other groups. These findings showed that the tensile strain at the fracture of scaffolds containing GTA crosslinker (GTA and TPP + GTA) was the smallest among all (Fig. 4g), which is in accordance with the fact that the GTA-crosslinked scaffolds usually tended to be more brittle, thus easy to fracture. The GP-crosslinked scaffold (0.14 ± 0.01 MPa) showed the lowest mechanical strength among all groups. In addition, the TPP + GTA-crosslinked scaffold exhibited distinctly higher Young's modulus than

the other crosslinked scaffolds (Fig. 4h), with a value of 11.8 ± 0.45 MPa. The Young's modulus of the scaffolds crosslinked with GTA, GP, TPP, and TPP + GP were 8.1 ± 0.35, 0.68 ± 0.12, 3.09 ± 0.64, and 2.1 ± 0.38 MPa, respectively. The GTA- and TPP + GTA-crosslinked scaffolds still showed the largest Young's modulus, since the GTA-crosslinked scaffolds were more brittle than the other groups. To sum up, the GTA- and TPP + GTA-crosslinked E/C-G composite scaffolds exhibited excellent mechanical strength but poor tensile strain due to the crosslinking properties of GTA, limiting its applicability in tissue engineering. For the GP-crosslinked E/C-G composite scaffolds, although previous studies had shown that GP is more eco-friendly and less biohazardous than GTA, the crosslinked scaffold presented low tensile stress and Young's modulus. However, the TPP- and TPP + GP-crosslinked scaffold not only showed sufficient mechanical strength, but also presented excellent mechanical toughness (adequate elongation), which can provide good mechanical support for soft-tissue ingrowth.

Wettability and swelling ratio

The wettability of printed tissue-engineering scaffolds is a critical parameter in the evaluation of their biological properties, since it determines its hydrophobicity or hydrophilicity that could affect protein, cell and tissue adhesion, and growth [27, 41]. The wettability of the E/C-G composite scaffolds crosslinked using different methods was analyzed by contact angle measurement using a goniometer, including measurements at the outer surface and the cross sections of the scaffolds. The results of water contact angle measurement of the crosslinked scaffolds are shown in Figs. 5a and 5b. For the outer surface of the scaffolds, the water contact angle of all tested groups was less than 90°, and the angle value of GTA-, GP-, TPP-, TPP + GTA-, and TPP + GP-crosslinked scaffold was 71.1°, 86.6°, 62.8°, 63.6°, and 73.3°, respectively. The water contact angle of the TPP-crosslinked scaffold was the smallest among all, which means that this scaffold was more hydrophilic. For the cross sections of the crosslinked scaffolds, the water contact angle of all tested groups was decreased in comparison with those at the outer surface of the crosslinked scaffold; the value of GTA-, GP-, TPP-, TPP + GTA-, and TPP + GP-crosslinked scaffold was 28.8°, 46.3°, 35.1°, 28.6°, and 30.8°, respectively. Figure 5b clearly proves that the water contact angle of the cross section of the crosslinked scaffolds was lower than that of the outer surface, which might be caused by the complete crosslinking of the scaffold surface.

The swelling capacity of a tissue-engineering scaffold is one of the most important factors to investigate its potential for tissue-engineering applications. The swelling curves of the differently crosslinked E/C-G composite scaffolds as a function of time in PBS and DME/F-12 culture medium at 37 °C are shown in Figs. 5c–5h. The mass swelling curves of the crosslinked scaffolds in PBS and DME/F-12 are shown in Figs. 5c and 5d, showing that the swelling ratio of all scaffolds increased over time. However, after 60 min of swelling, the increasing trend of swelling rate became flat and then remained unchanged. The mass swelling ratio of the GTA-crosslinked scaffold was the lowest among all scaffolds immersed in both PBS and DME/F-12, followed by the TPP + GTA crosslinked group, which might cause the higher crosslinking degree caused by GTA. However, the GP-, TPP-, and TPP + GP-crosslinked scaffolds showed remarkable swelling properties. Swelling ability is considered an essential element for the evaluation of scaffolds for tissue engineering and regenerative medicine, as it greatly determines cell growth, adhesion, and vascularization under in vivo conditions [54]. By comparing the swelling rates of the scaffolds treated with different crosslinkers in PBS and DME/F-12 (Fig. 5e), the swelling ratio in PBS was obviously higher than that in the DME/F-12 culture medium. The swelling of filament size is also an essential parameter for evaluating scaffold fidelity, as it affects the pore size. The size swelling ratios of differently crosslinked filaments were measured for 60 min in PBS and DME/F-12, as shown in Figs. 5f and 5g. In the PBS solution, all filaments presented a distinct increase in size swelling ratio over the first 10 min, increased more steadily afterward, and then maintained an equilibrium. Similar to the results of the mass swelling ratio of scaffolds, the size swelling ratio of GP-crosslinked filaments was the highest among all groups, with the maximum value of (69.1 ± 0.5)%, which is in accordance with the shrinkage results of the scaffolds (Fig. 4c). The GTA-crosslinked filaments showed the lowest size swelling ratio at (37.5 ± 0.2)%. The size swelling ratio of the TPP-, TPP + GP-, and TPP + GTA-crosslinked filaments lied between that of the GTA and GP groups. In the DME/F-12 culture medium, the size swelling ratio of all filaments showed a rapid increase over the first 20 min, then increased more steadily, and remained unchanged later. Similar with PBS but not identical is that the GP-crosslinked filaments showed the largest swelling ratio ((48.5 ± 0.8)%), and the GTA group exhibited the lowest ((28.6 ± 0.5)%). The maximum values of size swelling ratio of all filaments in PBS were observed to be greater than in DME/F-12 culture medium (Fig. 5h). These results indicated that all of the crosslinked scaffolds possess an excellent water absorption ability, which is in accordance with the water contact angle measurement results. Moreover, the comparison of the volume and size of scaffolds before and after swelling revealed that the slight additional swelling of all scaffolds had no significant impact on the feature resolution of the printed scaffolds; therefore, different crosslinking methods can be applied to prepare tissue-engineering scaffolds according to the requirements of native tissues or organs.

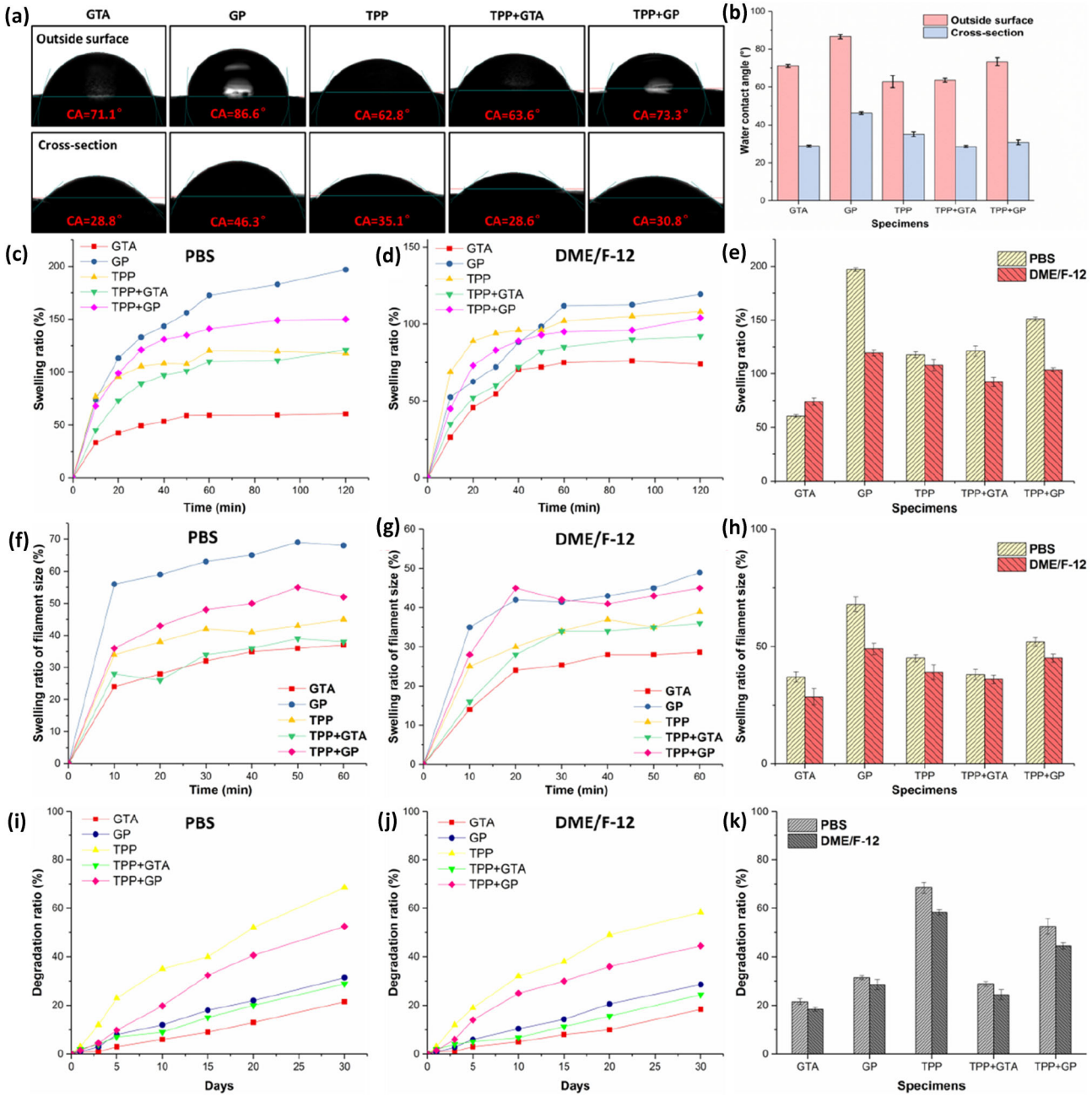

Fig. 5 Physical characteristics of the differently crosslinked E/C-G composite scaffolds. **a** Appearance of water contact angle on the outer surface and cross section of scaffolds; **b** statistics of water contact angle; **c** mass swelling curves in PBS and **d** in DME/F-12; **e** statistics of the mass swelling ratio in PBS and DME/F-12; **f** the swelling curves of filaments during 60 min of soaking in PBS and **g** in DME/F-12; **h** statistics of the swelling ratio of filament size in PBS and DME/F-12; the degradation curves for 30 days in **i** PBS and **j** in DME/F-12; and **k** statistics of degradation ratio in PBS and DME/F-12; the error bars represent the standard deviation ($n = 3$)

Degradation rate

The stability of tissue-engineering scaffolds is a key factor affecting the growth of cells or tissue, as it should provide a supportive environment for long-term stable cell adhesion. Thus, a static degradation experiment was carried out to test the stability of the differently crosslinked scaffolds in PBS and DME/F-12 at 37 °C. The degradation ratio (i.e., mass loss) of the differently crosslinked E/C-G composite scaffolds was measured over 30 days, with the obtained values shown in Figs. 5i–5k. The degradation ratios of all groups increased with time when immersed both in PBS and DME/F-12 (Figs. 5i and 5j). In the PBS solution, the GTA-crosslinked scaffolds exhibited the lowest degradation rate among all

groups, and the value reached (21.5 ± 1.2)% at day 30. However, the degradation ratio of the TPP-crosslinked scaffolds was the highest, with (68.5 ± 2.2)% at day 30. The degradation ratio of the scaffolds crosslinked with TPP + GTA, TPP + GP, and GP was (28.9 ± 0.91)%, (52.5 ± 3.2)%, and (31.4 ± 0.8)%, respectively. In the DME/F-12 culture medium, similar to the results in PBS solution, the TPP-crosslinked scaffold showed the highest degradation rate with (58.3 ± 1.1)% at day 30, while the GTA-crosslinked scaffolds had the lowest degradation rate with (18.4 ± 0.8)% at day 30. The degradation ratios of the scaffolds crosslinked with TPP + GTA, TPP + GP, and GP were (24.4 ± 2.1)%, (44.5 ± 1.3)%, and (28.6 ± 2.1)%, respectively. The comparison of the degradation ratio of scaffolds in PBS and DME/F-12 (Fig. 5k) showed that the degradation rate of all groups was higher in PBS than DME/F-12. This observation was in accordance with the results of swelling and crosslinking degree, which means that the stability of the scaffolds can be adjusted by the crosslinking degree: the higher the crosslinking degree, the lower the degradation rate.

Cell viability and proliferation assay

The cytocompatibility of tissue-engineering scaffolds is an essential factor to evaluate the feasibility of their clinical application. To evaluate this parameter for the fabricated E/C-G composite scaffolds, HUVECs were seeded on the surface of the differently crosslinked scaffolds, cultured for 4 days, and stained for live/dead cell assay. The fluorescence images of live/dead-stained cells and the quantitative statistics of cell viability are shown in Fig. 6. The viability of cells seeded onto the TPP + GP-crosslinked scaffolds was the highest among all scaffolds with a value of (98.7 ± 0.5)% on day 4. The surface of the TPP + GP-crosslinked scaffolds was totally covered by homogeneously distributed live cells, and almost no dead cells were found. A similar result was found for TPP-crosslinked scaffolds: the cell viability here was (91.5 ± 0.7)% on day 4. The fluorescence images of the live/dead cell staining on TPP-crosslinked scaffolds exhibited high viability, whereas only a few dead cells were found. Meanwhile, the GTA-crosslinked scaffolds presented the lowest cell viability among all observed conditions, as the value was (52.6 ± 2.8)% for HUVECs on day 4. In addition, plenty of the dead cells were found on the surface of these scaffolds. The TPP + GTA dual crosslinked scaffolds also exhibited poor cell viability on day 4 with a value of (71.1 ± 3.4)%, and many dead cells are present. The comparison of cell viability results for TPP-, GTA-, and TPP + GTA-crosslinked scaffolds demonstrated that the cell viability of HUVECs was decreased due to the cytotoxicity of the GTA crosslinking agent. Previous studies have reported that the GTA crosslinker inhibited cell viability and proliferation due to its greater cytotoxicity [51, 52]. As reported previously [53], although the GTA residues in the crosslinked scaffold can be washed out with excess water or blocking the residual aldehyde groups with glycine to reduce the GTA-associated toxicity, the cell viability of the crosslinked scaffold was still low after such a post-crosslinking treatment. In this study, the GP-crosslinked scaffolds also presented excellent cell viability for HUVECs with a value of (81.4 ± 1.2)%. However, the cell viability of the TPP-crosslinked scaffolds was higher than that of the GP-crosslinked ones under the same conditions. In addition, the fluorescent live/dead cell staining results showed that HUVECs could maintain higher cell viability on the TPP-crosslinked scaffolds than the GP-crosslinked ones. Meanwhile, although the GP-crosslinked scaffolds promoted high cell viability, the high cost of GP limits making use of its universal benefits and massive production. Altogether, these results confirmed that the TPP-, GP-, and TPP + GP-crosslinked E/C-G composite scaffolds featured favorable cytocompatibility and non-toxicity, and the TPP- and TPP + GP-crosslinked scaffolds presented higher cell viability and vascular cell responsiveness.

In order to further demonstrate the effects of TPP and TPP + GP crosslinking on cell viability and morphology, HUVECs were seeded on the surface of the E/C-G composite scaffolds. The morphology of adhered cells was observed and live/dead cell detection was performed to analyze the viability of HUVECs on the scaffolds directly after seeding (day 0) and after culture for 2 and 4 days (Figs. 7 and 8). It could be seen that the cells remained highly viable when they were seeded on the TPP-crosslinked scaffolds (Fig. 7a). After culturing for 2 days, the cells maintained high viability, and their number obviously increased, even though a few dead cells could be found in the corresponding image of dead cells. On day 4, the scaffolds were covered by homogeneously distributed HUVECs, and strands appeared as wrappings by a layer of cells (also, a video was captured to show cell adhesion on the entire 3D surface of the scaffold in different focal planes, as shown in Video S1 in Supplementary Information; magnification: 4×), which indicates the vascular cell responsiveness in contact with the TPP-crosslinked E/C-G composite scaffolds. Moreover, Fig. 7b shows that the surface of the scaffold was covered with cells, and the cells even grew into the pores between the filaments. The microscopic images with higher magnification demonstrate that cell sprouts and primitive cell networks were formed in the pore structures between adjacent filaments (Figs. 7c and 7d). Furthermore, immune fluorescent staining of the scaffold was carried out to visualize the cell cytoskeleton and nuclei for the observation of cell morphology in the scaffolds after 4 days of culture. The TRITC − phalloidin and DAPI staining (Figs. 7e–7g) show the high cell density throughout the surface of the scaffolds, and the magnified images show that the cells maintained their normal phenotypes and became flat in

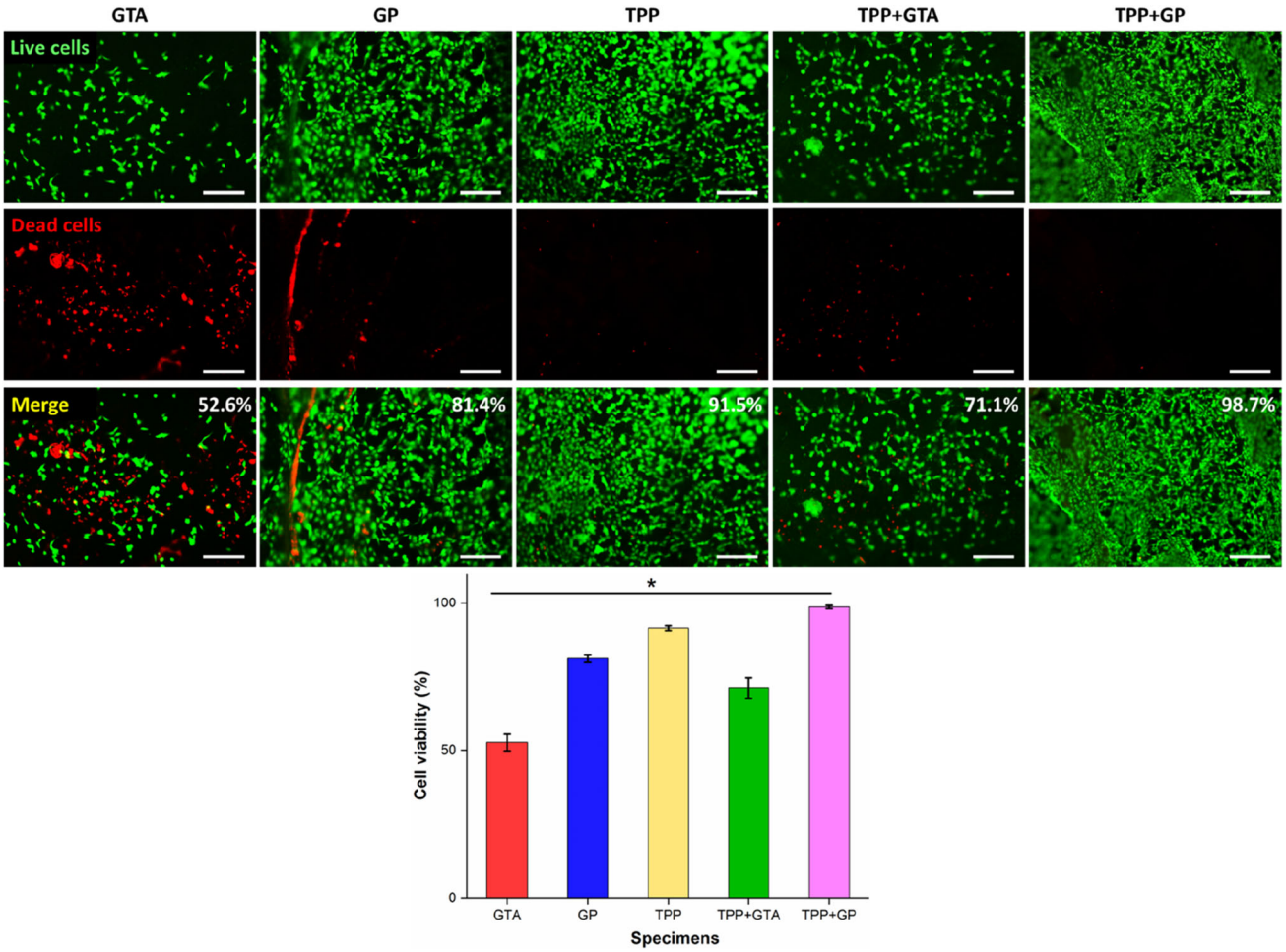

Fig. 6 Biocompatibility assay of the differently crosslinked E/C-G composite scaffolds with HUVECs after 4 days of culture: representative live/dead staining images and cell viability based on the count of dead and live cell numbers; scale bars: 500 μm; the error bars represent the standard deviation ($n = 3$), and a value of $^{*}p \leq 0.05$ was considered statistically significant

appearance, which is the native form of HUVECs. The high-magnification images demonstrate defined actin fibers and round nuclei (Figs. 7f and 7g) in a growing number of cells, which indicate cell migration and active cell division. To quantify the cell spreading phenomenon, the coverage rate of live cells on the surface of scaffolds was determined in correspondence with live/dead fluorescence images (Fig. 7a) after culture for 0, 2, and 4 days. The results demonstrated that the coverage of live cells on the scaffolds increased from (41.5 ± 2.3)% (attachment at 4 h) to (92.89 ± 3.9)% after 4 days of culture (Fig. 7h). Moreover, the morphology of cells growing on the scaffolds was evaluated by SEM after 2 and 4 days, as shown in Figs. 8a–8h. The TPP-crosslinked scaffolds and TPP + GP-crosslinked scaffolds were investigated in this regard. In the TPP-crosslinked scaffolds group, cells adhered onto the surface of scaffolds with a close cell-to-cell contact after 2 days of culture (Fig. 8a), and cellular networks could be observed at different levels of magnification (Fig. 8a1). By day 4, the number of cells had increased obviously, and the scaffolds were almost covered (Fig. 8b) with a homogeneous monolayer of cells formed on the scaffold surface (Fig. 8b1). Similar results were found in the TPP + GP-crosslinked scaffolds, as shown in Figs. 8c, 8c1, 8d, and 8d1: a dense layer of cells adhered onto the surface of scaffolds. Meanwhile, the coverage rate of cells on the surface of scaffolds was quantitatively analyzed according to the obtained SEM images (Figs. 8a–8d). The value of coverage rate of the two groups increased with culture time from (48.3 ± 2.1)% (day 2) to (89.6 ± 1.5)% (day 4) in the TPP-crosslinked scaffolds and from (54.1 ± 3.2)% (day 2) to (92.8 ± 2.1)% (day 4) in the TPP + GP-crosslinked scaffolds. These results corresponded with those of the live/dead cell staining. Moreover, the increased magnification (Figs. 8e and 8f) revealed that the cells were well-spread on the surface with cell-to-cell connections showing filopodia-like morphology (Fig. 8f, indicated by a yellow arrow). Figure 8g depicts that ring-shaped cell-to-cell interactions were established resulting in the formation of a rather dense cellular

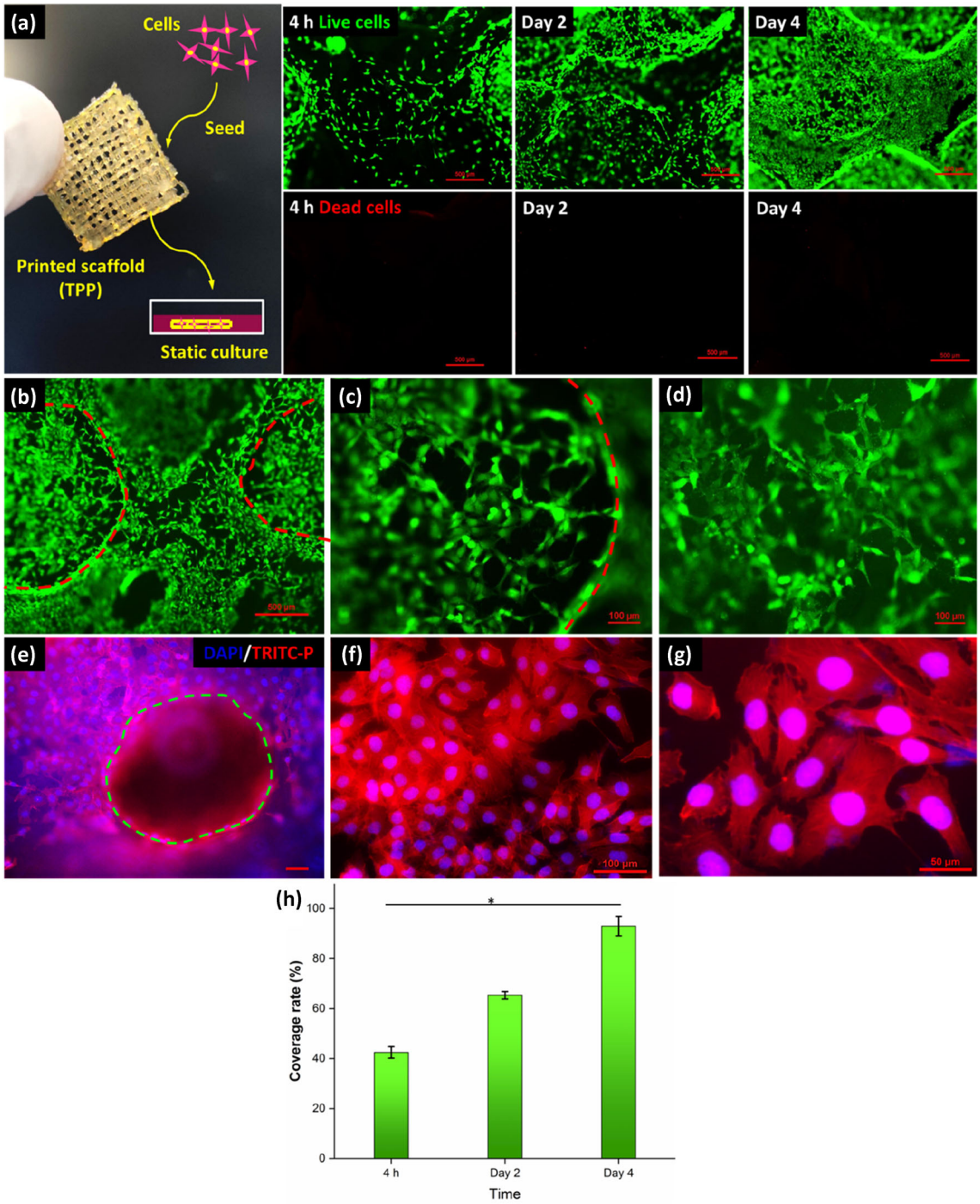

Fig. 7 **a** Representative fluorescent images of live/dead HUVECs cultured on the TPP-crosslinked E/C-G composite scaffold after 0 (4 h of adhesion), 2 and 4 days; **b** pore structure of cell-seeded scaffold (the red lines present the edge of filaments); **c**, **d** the highly magnified microscopic images: cell sprout formation and primitive cell networks were formed in the pores between adjacent filaments; **e**–**g** fluorescent microscopic images of cell nuclei (DAPI, blue) and actin cytoskeleton (TRITC − P, red) on the surface of E/C-G composite scaffolds after 4 days; scale bars: (**e**, **f**) 100 μm, **g** 50 μm; **h** the coverage rate of live cells on the surface of scaffolds in correspondence with the live/dead fluorescent images (**a**); a value of $*p \leq 0.05$ was considered statistically significant

network on the surface and inside the macropores of the scaffold (Fig. 8h). Overall, these results indicated that HUVECs can adhere, proliferate, and migrate on the TPP- and TPP + GP-crosslinked E/C-G composite scaffolds, allowing the formation of a "pre-vascular" network by these vascular cells.

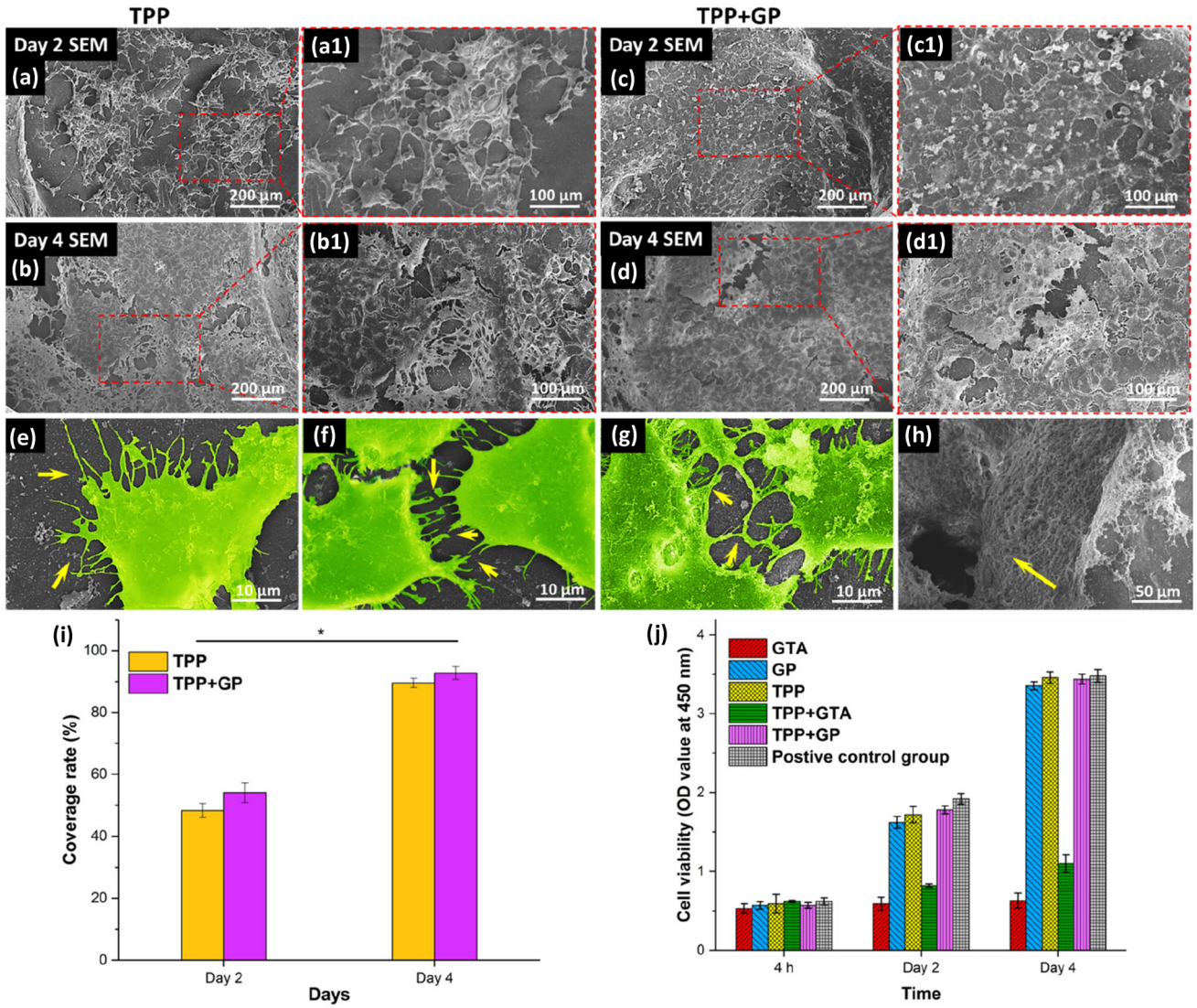

Fig. 8 **a**–**h** SEM micrographs of HUVECs attached to the surface of the TPP- and TPP + GP-crosslinked E/C-G composite scaffolds after 2 and 4 days of culture: (**a**, **a1**) 2 days and (**b**, **b1**) 4 days on the TPP-crosslinked scaffold, (**c**, **c1**) 2 days and (**d**, **d1**) 4 days on the TPP + GP-crosslinked scaffold, (**e**, **f**) higher magnification of SEM images of the TPP-crosslinked scaffold after 4 days (the yellow arrows indicate formed filopodia of cells), (**g**, **h**) same of TPP + GP-crosslinked scaffolds; (**i**) the cell coverage rate on TPP- and TPP + GP-crosslinked scaffolds after 2 and 4 days in correspondence with (**a**–**d**); (**j**) CCK-8 assay data analysis of cultivation of HUVECs after 0 (4 h of adhesion), 2 and 4 days. The error bars represent the standard deviation ($n = 3$) and a value of $^{*}p \leq 0.05$ was considered statistically significant

In order to further understand the activity of HUVECs and quantitatively analyze the possible cytotoxicity of the differently crosslinked E/C-G composite scaffolds, cell proliferation was investigated by using CCK 8 assay after culture for 0, 2, and 4 days under the same conditions. The results of the CCK 8 assay are shown in Fig. 8j. The results obviously indicate that the optical density (OD) value of the GTA-crosslinked scaffolds hardly increased with culturing time, and that of the TPP + GTA-crosslinked scaffolds showed a small increase at day 4 only (absorbance of 1.1, compared to 0.82 at day 2, i.e., a 1.34-fold increase, $p < 0.05$). These results were in agreement with the live/dead cell staining results, which further indicated that the GTA-crosslinked scaffolds maintained greater cytotoxicity that is not conducive to cell growth. On the contrary, the GP-, TPP-, and TPP + GP-crosslinked scaffolds showed an increase in cell numbers over time. In the GP-crosslinked group, the absorbance value increased from 1.62 on day 2 to 3.35 on day 4, equivalent to a 2.06-fold increase ($p < 0.05$). The absorbance value of the TPP-crosslinked scaffold increased from 1.69 on day 2 to 3.46 on day 4 (2.05-fold increase, $p < 0.05$). In the TPP + GP-crosslinked group, the absorbance value increased from

1.72 on day 2 to 3.45 on day 4, i.e., a 2.01-fold increase ($p < 0.05$). The positive trends of absorbance in these three experimental groups were consistent with the positive development of cell numbers in the control group (polystyrene surface of the well plate). The results correlated well with the previously observed live/dead cell assay data. The increase in absorbance value is a direct measure of cell metabolic activity rate within different culture environments. Therefore, these results indicated that the TPP-crosslinked E/C-G composite scaffolds exhibited the best favorable cytocompatibility and non-cytotoxicity, followed by the GP-crosslinked E/C-G composite scaffolds; the GTA-crosslinked scaffolds maintained greater cytotoxicity, which is not conducive to tissue-engineering applications.

Angiogenic potential of E/C-G composite scaffolds

In order to preliminarily verify our original hypothesis, we applied a CAM assay, a well-established model to investigate the angiogenic potential of scaffolds. The prepared scaffolds were implanted onto the top of embryo chorioallantoic membrane for cultivation, as shown in Fig. 9a. Seven days after insertion of the scaffolds onto the CAM (i.e., 14 days after start of the experiments), neo-vessels formed in the upper surface and pores of E/C-G composite scaffolds (TPP-crosslinked), shown by micrographs shown in Figs. 9b and 9b1; the control group of C-G scaffold (TPP-crosslinked) is shown in Figs. 9c and 9c1 for comparison. The results clearly exhibited that lots of neo-vessels could grow under the scaffolds in both groups, which means that these two scaffolds were non-toxic. We found many newly formed vessels grew into the pores of the scaffolds and spread on their upper surface in the E/C-G composite scaffold group (Fig. 9b1, yellow arrows), which was not observed in the C-G composite scaffold group. After the fixation of harvested samples, micrographs of the lower surface of the scaffolds were taken, as shown in Fig. 9b2 (E/C-G composite scaffold group) and Fig. 9c2 (C-G composite scaffold group), to count the number of newly formed blood vessels. A number of representative neo-vessel images were processed by using ImageJ software, as shown in Fig. 9b3 (E/C-G composite scaffold group) and Fig. 9c3 (C-G composite scaffold group), and the total number of vessels was also quantified, with the results presented in Fig. 9d. The number of vessels in the E/C-G composite scaffold group was significantly higher than that in the C-G composite scaffold group. Moreover, H&E and Masson staining of the paraffin-embedded CAMs revealed that these two scaffolds were able to be incorporate into the host tissue, and new tissue could grow into the pores of the respective scaffolds (Figs. 9e–9h). Many neo-vessels were formed and grew into the pores of the E/C-G composite scaffolds (Figs. 9e and 9f, red arrows), but these were seldom found in the C-G composite scaffolds (Figs. 9g and 9h, red arrows). In view of the above results, we could preliminary verify our hypothesis that the printed scaffolds consisting of E/C-G composite hydrogel have a certain potential to promote angiogenesis. However, in this work, neo-vessels could only grow on the surface and pores of scaffolds but not inside of the printed material strands. Moreover, due to the time limitation (up to 21 days) of the CAM assay, it was not possible to further test the growth of neo-vessels; an animal model (e.g., subcutaneous implantation in rats) should be applied in future work to evaluate the capability of E/C-G composite scaffolds for angiogenesis and their biocompatibility.

Conclusions

In this study, multi-material composite hydrogels consisting of chitosan, gelatin, and egg white (E/C-G) were investigated and optimized as potential biomaterials for 3D printing applications by systematically studying the relevant factors for tissue-engineering (TE) application. An optimal formulation of E/C-G hydrogel (E/C-G ratio = 2:8) was determined by a set of systematic quantitative characterization tests. Flowability and rheological tests, filament fusion, and collapse tests were conducted to validate the printability and shape fidelity of the fabricated scaffold. The findings revealed that this blend exhibited good printability and shape fidelity for the fabrication of intended scaffolds, and thus was suitable for the 3D extrusion printing of tissue-engineering scaffolds. Then, a series of comparative analyses of various crosslinking methods were performed to stabilize the printed E/C-G composite scaffolds. Three crosslinking agents (GTA, GP, and TPP) and five crosslinking methods (GTA, GP, TPP, TPP + GTA, and TPP + GP) were applied to investigate their applicability for the E/C-G composite hydrogel. The differently crosslinked E/C-G scaffolds were prepared and evaluated for physical and biological characteristics, including shrinkage ratio, porosity, crosslinking degree, mechanical properties, hydrophilicity, swelling ratio, degradation, and biocompatibility. The results showed that all groups of crosslinked scaffolds presented high porosity, and good hydrophilicity and swelling properties. The GTA- and TPP + GTA-crosslinked scaffolds exhibited satisfactory crosslinking degree and mechanical strength, but showed obvious friability (poor elongation) and certain levels of cytotoxicity, i.e., GTA proved as useful in physicochemical terms but poor concerning cytocompatibility. The GP-, TPP-, and TPP + GP-crosslinked scaffolds exhibited better biocompatibility than the other groups, while the TPP- and TPP + GP-crosslinked scaffolds showed superior mechanical properties as compared to the GP-treated group. The TPP (single crosslinking) and TPP + GP (two-step crosslinking) exhibited similar results, not to mention that it is more cost-effective than GP. Taken together, TPP is recommended as the

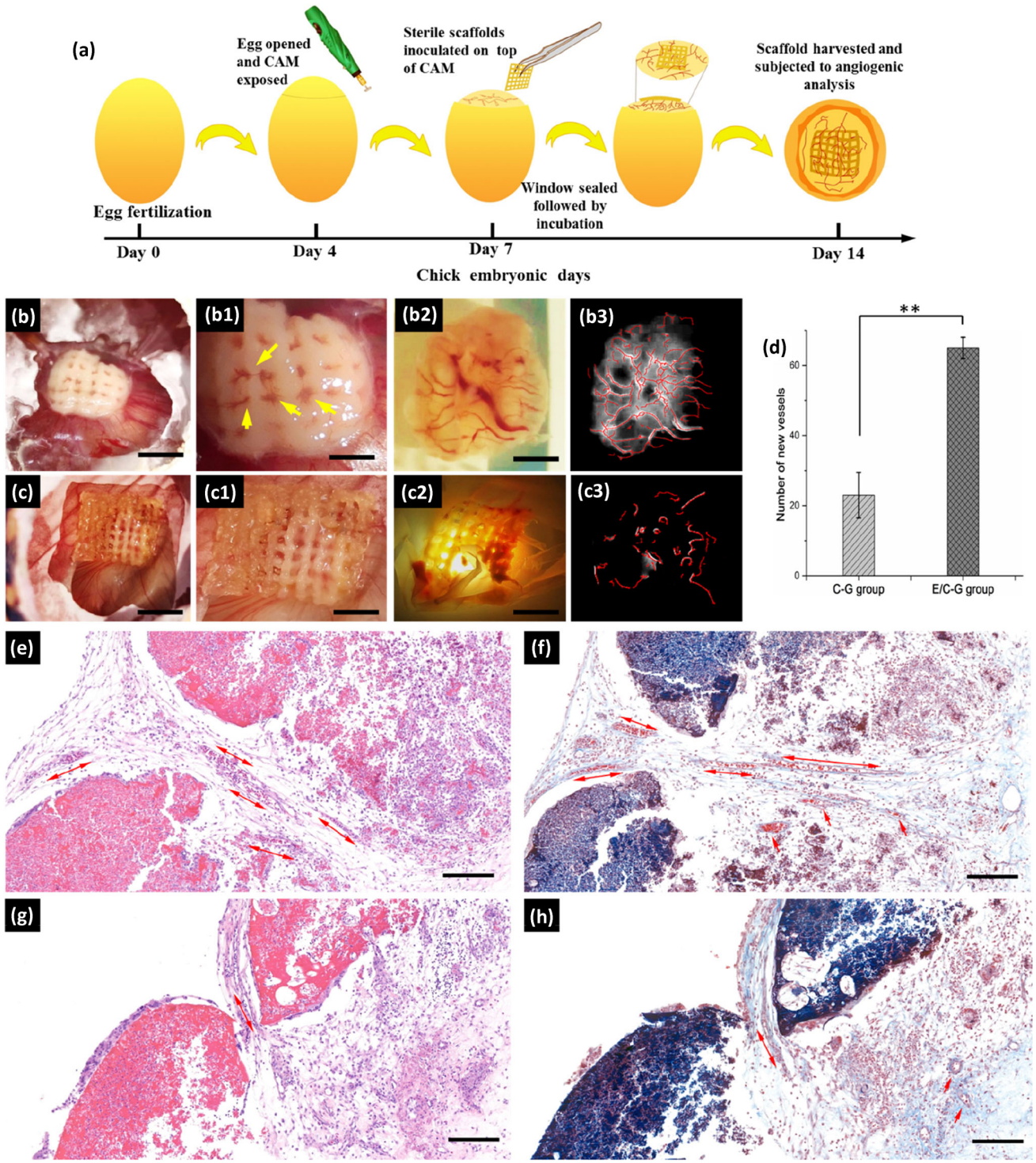

Fig. 9 Biocompatibility and in vivo angiogenic potential of the E/C-G composite scaffold and C-G composite scaffold; **a** schematic representation of the implantation of scaffold onto the CAM; **b**–**b3** E/C-G composite scaffold group: **b**, **b1** micrographs of neo-vessels in the upper surface and pores of the scaffold (the yellow arrows indicate neo-vessels), **b2** micrograph of neo-vessels on the lower surface of scaffolds, **b3** neo-vessel image processed by ImageJ software corresponding with **b2**, scale bar: 10 mm; **c**–**c3** C-G composite scaffold group corresponding with **b**–**b3**, scale bar: 10 mm; **d** quantification of the newly formed vessels in the harvested scaffold after 14 days; **e**–**h** images showing the H&E and Masson staining of paraffin-embedded CAMs: **e**, **f** E/C-G composite scaffold, **g**, **h** C-G composite scaffold (the red arrows indicate the neo-vessels), scale bar: 100 μm. The error bars represent the standard deviation ($n = 3$) and a value of $^{**}p \leq 0.01$ was considered statistically significant

most suitable crosslinker for the fabrication of E/C-G composite scaffolds. Finally, an in vitro cell experiment and an in vivo CAM assay were applied to evaluate the biological functionality of the E/C-G composite scaffolds. We found that HUVECs not only maintained high viability and proliferation, but also presented cell sprout formation and the organization of cellular networks; also, compared to the C-G composite scaffolds without egg white, E/C-G composite scaffolds could support the growth of new vessels into the pores of the scaffold, easily forming connections with the host tissue for transporting oxygen and nutrients to the center of the scaffold. In conclusion, the results of this study imply that E/C-G composite hydrogel and the 3D printed scaffolds thereof have great potential for TE applications. In future work, the angiogenesis capability of E/C-G composite scaffolds will be further evaluated and applied to 3D printing cell-free and cell-laden cardiac patches.

Supplementary Information The online version contains supplementary material available at https://doi.org/10.1007/s42242-022-00194-3.

Acknowledgements The authors acknowledge the funding support from the National Natural Science Foundation of China (Nos. 52175474 and 51775324) and the China Scholarship Council (No. 202006890054). The authors acknowledge the valuable comments and time spent by referees to improve this manuscript.

Author contributions SL was involved in conceptualization, data curation, methodology, investigation, writing–review and editing, and visualization; HZ and YL contributed to formal analysis and review and editing; TA, DK, and MG contributed in validation, review and editing, and supervision. QH contributed to funding acquisition and supervision.

Funding Open Access funding enabled and organized by Projekt DEAL.

Declarations

Conflict of interest The authors declare that there is no conflict of interest.

Ethical approval This article does not contain any studies with human or animal subjects performed by any of the authors.

Open Access This article is licensed under a Creative Commons Attribution 4.0 International License, which permits use, sharing, adaptation, distribution and reproduction in any medium or format, as long as you give appropriate credit to the original author(s) and the source, provide a link to the Creative Commons licence, and indicate if changes were made. The images or other third party material in this article are included in the article's Creative Commons licence, unless indicated otherwise in a credit line to the material. If material is not included in the article's Creative Commons licence and your intended use is not permitted by statutory regulation or exceeds the permitted use, you will need to obtain permission directly from the copyright holder. To view a copy of this licence, visit http://creativecommons.org/licenses/by/4.0/.

References

1. Ouyang L, Armstrong JPK, Lin Y et al (2020) Expanding and optimizing 3D bioprinting capabilities using complementary network bioinks. Sci Adv 6(38):eabc5529. https://doi.org/10.1126/sciadv.abc5529
2. Moroni L, Burdick JA, Highley C et al (2018) Biofabrication strategies for 3D in vitro models and regenerative medicine. Nat Rev Mater 3(5):21–37. https://doi.org/10.1038/s41578-018-0006-y
3. Lode A, Meissner K, Luo Y et al (2015) Fabrication of porous scaffolds by three-dimensional plotting of a pasty calcium phosphate bone cement under mild conditions. J Tissue Eng Regen Med 8(9):682–693. https://doi.org/10.1002/term.1563
4. Lee SC, Gillispie G, Prim P et al (2020) Physical and chemical factors influencing the printability of hydrogel-based extrusion bioinks. Chem Rev 120(19):10834–10886. https://doi.org/10.1021/acs.chemrev.0c00015
5. Huyer LD, Montgomery M, Zhao Y et al (2015) Biomaterial based cardiac tissue engineering and its applications. Biomed Mater 10(3):034004. https://doi.org/10.1088/1748-6041/10/3/034004
6. Bedell ML, Navara AM, Du Y et al (2020) Polymeric systems for bioprinting. Chem Rev 120(19):10744–10792. https://doi.org/10.1021/acs.chemrev.9b00834
7. Leberfinger AN, Dinda S, Wu Y et al (2019) Bioprinting functional tissues. Acta Biomater 95:32–49. https://doi.org/10.1016/j.actbio.2019.01.009
8. De Maria C, Vozzi G, Moroni L (2017) Multimaterial, heterogeneous, and multicellular three-dimensional bioprinting. MRS Bull 42:578–584. https://doi.org/10.1557/mrs.2017.165
9. Jiang T, Munguia-Lopez JG, Gu K et al (2019) Engineering bioprintable alginate/gelatin composite hydrogels with tunable mechanical and cell adhesive properties to modulate tumor spheroid growth kinetics. Biofabrication 12(1):015024. https://doi.org/10.1088/1758-5090/ab3a5c
10. Ahmed EM (2015) Hydrogel: Preparation, characterization, and applications: a review. J Adv Res 6(2):105–121. https://doi.org/10.1016/j.jare.2013.07.006
11. Keane TJ, Badylak SF (2014) Biomaterials for tissue engineering applications. Semin Pediatr Surg 23(3):112–118. https://doi.org/10.1053/j.sempedsurg.2014.06.010
12. Banyard DA, Bourgeois JM, Widgerow AD et al (2015) Regenerative biomaterials: a review. Plast Reconstr Surg 135(6):1740–1748. https://doi.org/10.1097/prs.0000000000001272
13. Chimene D, Kaunas R, Gaharwar AK (2020) Hydrogel bioink reinforcement for additive manufacturing: a focused review of emerging strategies. Adv Mater 32(1):e1902026. https://doi.org/10.1002/adma.201902026
14. Habib A, Sathish V, Mallik S et al (2018) 3D printability of alginate-carboxymethyl cellulose hydrogel. Materials 11(3):454. https://doi.org/10.3390/ma11030454
15. Schütz K, Placht AM, Paul B et al (2017) Three-dimensional plotting of a cell-laden alginate/methylcellulose blend: towards biofabrication of tissue engineering constructs with clinically relevant dimensions. J Tissue Eng Regen Med 11(5):1574–1587. https://doi.org/10.1002/term.2058
16. Ahlfeld T, Cidonio G, Kilian D et al (2017) Development of a clay based bioink for 3D cell printing for skeletal application. Biofabrication 9(3):034103. https://doi.org/10.1088/1758-5090/aa7e96
17. Erkoc P, Uvak I, Nazeer MA et al (2020) 3D printing of cytocompatible gelatin-cellulose-alginate blend hydrogels. Macromol Biosci 20(10):e2000106. https://doi.org/10.1002/mabi.202000106
18. Wang XF, Lu PJ, Song Y et al (2016) Nano hydroxyapatite particles promote osteogenesis in a three-dimensional bio-printing construct consisting of alginate/gelatin/hASCs. RSC Adv 6(8):6832–6842. https://doi.org/10.1039/c5ra21527g

19. Kumar M (2000) A review of chitin and chitosan applications. React Funct Polymers 46(1):1–27. https://doi.org/10.1016/S1381-5148(00)00038-9
20. Liu X, Ma L, Mao Z et al (2011) Chitosan-based biomaterials for tissue repair and regeneration. Chitosan Biomater II 244:81–127. https://doi.org/10.1007/12_2011_118
21. Croisier F, Jérôme C (2013) Chitosan-based biomaterials for tissue engineering. Eur Polymer J 49(4):780–792. https://doi.org/10.1016/j.eurpolymj.2012.12.009
22. Ng WL, Yeong WY, Naing MW (2016) Polyelectrolyte gelatin-chitosan hydrogel optimized for 3D bioprinting in skin tissue engineering. Int J Bioprint 2(1):10. https://doi.org/10.18063/ijb.2016.01.009
23. Du JR, Hsu LH, Xiao ES et al (2020) Using genipin as a "green" crosslinker to fabricate chitosan membranes for pervaporative dehydration of isopropanol. Separation Purif Technol 244:116843. https://doi.org/10.1016/j.seppur.2020.116843
24. Djabourov M, Leblond J, Papon P (1988) Gelation of aqueous gelatin solutions. I Struct Investig J Phys 49(2):319–332. https://doi.org/10.1051/jphys:01988004902031900
25. Djabourov M, Leblond J, Papon P (1988) Gelation of aqueous gelatin solutions. II. Rheology of the sol-gel transition. J Phys 49(2):333–343. https://doi.org/10.1051/jphys:01988004902033300
26. Fischetti T, Celikkin N, Contessi Negrini N et al (2020) Tripolyphosphate-crosslinked chitosan/gelatin biocomposite ink for 3D printing of uniaxial scaffolds. Front Bioeng Biotechnol 8:400. https://doi.org/10.3389/fbioe.2020.00400
27. Liu S, Zhang H, Hu Q et al (2020) Designing vascular supportive albumen-rich composite bioink for organ 3D printing. J Mech Behav Biomed Mater 104:103642. https://doi.org/10.1016/j.jmbbm.2020.103642
28. Liu S, Hu Q, Shen Z et al (2021) 3D printing of self-standing and vascular supportive multimaterial hydrogel structures for organ engineering. Biotechnol Bioeng 119(1):118–133. https://doi.org/10.1002/bit.27954
29. Pinto CF, Berger SB, Cavalli V et al (2015) Influence of chemical and natural cross-linkers on dentin bond strength of self-etching adhesives. Int J Adhesion Adhesives 60:117–122. https://doi.org/10.1016/j.ijadhadh.2015.04.008
30. Chung S, King MW (2011) Design concepts and strategies for tissue engineering scaffolds. Biotechnol Appl Biochem 58(6):423–438. https://doi.org/10.1002/bab.60
31. Koc FE, Altıncekic TG (2020) Investigation of gelatin/chitosan as potential biodegradable polymer films on swelling behavior and methylene blue release kinetics. Polymer Bull 78(6):3383–3398. https://doi.org/10.1007/s00289-020-03280-7
32. Yu SH, Wu SJ, Wu JY et al (2013) Tripolyphosphate cross-linked macromolecular composites for the growth of shape- and size-controlled apatites. Molecules 18(1):27–40. https://doi.org/10.3390/molecules18010027
33. Liu C, Liu YY, Li S et al (2017) Bioprinted chitosan and hydroxyapatite micro-channels structures scaffold for vascularization of bone regeneration. J Biomater Tissue Eng 7:28–34. https://doi.org/10.1166/jbt.2017.1535
34. Lien SM, Ko LY, Huang TJ (2010) Effect of crosslinking temperature on compression strength of gelatin scaffold for articular cartilage tissue engineering. Mater Sci Eng C 30:631–635. https://doi.org/10.1016/j.msec.2010.02.019
35. Fang Y, Zhang T, Song Y et al (2020) Assessment of various crosslinking agents on collagen/chitosan scaffolds for myocardial tissue engineering. Biomed Mater 15(4):045003. https://doi.org/10.1088/1748-605X/ab452d
36. Ma L, Gao C, Mao Z et al (2003) Thermal dehydration treatment and glutaraldehyde cross-linking to increase the biostability of collagen-chitosan porous scaffolds used as dermal equivalent. J Biomater Sci Polym Ed 14(8):861–874. https://doi.org/10.1163/156856203768366576
37. Kiyotake EA, Douglas AW, Thomas EE et al (2019) Development and quantitative characterization of the precursor rheology of hyaluronic acid hydrogels for bioprinting. Acta Biomater 95:176–187. https://doi.org/10.1016/j.actbio.2019.01.041
38. Niu Y, Chen KC, He T et al (2014) Scaffolds from block polyurethanes based on poly(varepsilon-caprolactone) (PCL) and poly(ethylene glycol) (PEG) for peripheral nerve regeneration. Biomaterials 35(14):4266–4277. https://doi.org/10.1016/j.biomaterials.2014.02.013
39. Liu S, Sun L, Zhang H et al (2021) High-resolution combinatorial 3D printing of gelatin-based biomimetic triple-layered conduits for nerve tissue engineering. Int J Biol Macromol 166:1280–1291. https://doi.org/10.1016/j.ijbiomac.2020.11.010
40. Entekhabi E, Haghbin Nazarpak M, Sedighi M et al (2020) Predicting degradation rate of genipin cross-linked gelatin scaffolds with machine learning. Mater Sci Eng C Mater Biol Appl 107:110362. https://doi.org/10.1016/j.msec.2019.110362
41. Liu SH, Zhang HG, Hu QX et al (2020) Development and evaluation of biomimetic 3D coated composite scaffold for application as skin substitutes. Macromol Mater Eng 305(3):1900848. https://doi.org/10.1002/mame.201900848
42. Liu SH, Zhang HG, Li S et al (2019) A facile strategy for fabricating tissue engineering scaffolds with sophisticated prevascularized networks for bulk tissue regeneration. Macromol Mater Eng 304(5):1800642. https://doi.org/10.1002/mame.201800642
43. Silva AS, Santos LF, Mendes MC et al (2020) Multi-layer pre-vascularized magnetic cell sheets for bone regeneration. Biomaterials 231:119664. https://doi.org/10.1016/j.biomaterials.2019.119664
44. Datta S, Das A, Sasmal P et al (2018) Alginate-poly(amino acid) extrusion printed scaffolds for tissue engineering applications. Int J Polymeric Mater Polymeric Biomater 69(2):65–72. https://doi.org/10.1080/00914037.2018.1539988
45. López-Marcial GR, Zeng AY, Osuna C et al (2018) Agarose-based hydrogels as suitable bioprinting materials for tissue engineering. ACS Biomater Sci Eng 4(10):3610–3616. https://doi.org/10.1021/acsbiomaterials.8b00903
46. Yao B, Hu T, Cui X et al (2019) Enzymatically degradable alginate/gelatin bioink promotes cellular behavior and degradation in vitro and in vivo. Biofabrication 11(4):045020. https://doi.org/10.1088/1758-5090/ab38ef
47. Ahlfeld T, Cubo-Mateo N, Cometta S et al (2020) A novel plasma-based bioink stimulates cell proliferation and differentiation in bioprinted, mineralized constructs. ACS Appl Mater Interf 12(11):12557–12572. https://doi.org/10.1021/acsami.0c00710
48. Li J, Wu C, Chu PK et al (2020) 3D printing of hydrogels: rational design strategies and emerging biomedical applications. Mater Sci Eng R Rep 140:100543. https://doi.org/10.1016/j.mser.2020.100543
49. Shankar KG, Gostynska N, Montesi M et al (2017) Investigation of different cross-linking approaches on 3D gelatin scaffolds for tissue engineering application: a comparative analysis. Int J Biol Macromol 95:1199–1209. https://doi.org/10.1016/j.ijbiomac.2016.11.010
50. Oh SH, Park IK, Kim JM et al (2007) In vitro and in vivo characteristics of PCL scaffolds with pore size gradient fabricated by a centrifugation method. Biomaterials 28(9):1664–1671. https://doi.org/10.1016/j.biomaterials.2006.11.024
51. Takigawa T, Endo Y (2006) Effects of glutaraldehyde exposure on human health. J Occupat Health 48(2):75–87. https://doi.org/10.1539/joh.48.75
52. Beauchamp ROJr, St Clair MB, Fennell TR, et al (1992) A critical review of the toxicology of glutaraldehyde. Crit Rev Toxicol 22(3–4):143–174. https://doi.org/10.3109/10408449209145322

53. Kikuchi M, Matsumoto HN, Yamada T et al (2004) Glutaraldehyde cross-linked hydroxyapatite/collagen self-organized nanocomposites. Biomaterials 25(1):63–69. https://doi.org/10.1016/S0142-9612(03)00472-1

54. McAndrews KM, Kim MJ, Lam TY et al (2014) Architectural and mechanical cues direct mesenchymal stem cell interactions with crosslinked gelatin scaffolds. Tissue Eng Part A 20(23–24):3252–3260. https://doi.org/10.1089/ten.tea.2013.0753